Supplementary Material

Co^{II} immobilized on aminated Fe_3O_4@Boehmite nanoparticles (Fe_3O_4@Boehmite-NH_2-Co^{II} NPs): a novel, inexpensive and highly efficient heterogeneous magnetic nanocatalyst for Suzuki–Miyaura and Heck–Mizoroki cross-coupling reactions in green media

Arezou Mohammadinezhad , Batool Akhlaghinia*

**Department of Chemistry, Faculty of Sciences, Ferdowsi University of Mashhad, Mashhad 9177948974, Iran.*

Experimental

General

The purity determinations of the products and the progress of the reactions were accomplished by TLC on silica gel polygram STL G/UV 254 plates (preparative TLC was carried out using a Merck GF 254 silica gel on a glass support) or column chromatography on silica gel 60 (230-400 mesh) and GC-17A Shimadzu device.. The melting points of the products were determined with an Electrothermal Type 9100 melting point apparatus. The FT-IR spectra were recorded on pressed KBr pellets using an AVATAR 370 FT-IR spectrometer (Therma Nicolet spectrometer, USA) at room temperature in the range between 4000 and 400 cm^{-1} with a resolution of 4 cm^{-1}. The NMR spectra were provided by Brucker Avance 300, 400 and 500 MHz instruments in $CDCl_3$ in the presence of tetramethylsilane as the internal standard and the coupling constants (*J* values) are given in Hz. Elemental analyses were performed using a Thermo Finnigan Flash EA 1112 Series instrument (furnace: 900 ˚C, oven: 65 ˚C, flow carrier: 140 mL min^{-1}, flow reference: 100 mL min^{-1}). Mass spectra were recorded with a CH7A Varianmat Bremem instrument at 70 eV electron impact ionization, in *m/z* (rel%). X-ray powder diffraction (XRD) was performed on a PANalytical Company X'Pert Pro MPD diffractometer with Cu Ka radiation ((λ = 0.154 nm) radiation. BET surface area and pore size distribution were measured on a Belsorp mini II system at –196˚ C using N_2 as the adsorbate. Transmission electron microscopy (TEM) was performed with a Leo 912 AB (120 kV) microscope (Zeiss, Germany). FE-SEM images were recorded using a TESCAN, Model: MIRA3 scanning electron microscope operating at an acceleration voltage of 30.0 kV (manufactured by the Czech Republic). Elemental compositions were determined with an SC7620 energy-dispersive X-ray analysis (EDX) presenting a 133 eV resolution at 20 kV. Thermogravimetric analyses (TGA and DTG) were carried out using a Shimadzu Thermogravimetric Analyzer (TG-50) in the temperature range of 25–950 ˚C at a heating rate of 10˚C min^{-1}, under air atmosphere. Hydrogen temperature-programmed reduction (H_2-TPR) was carried out using a Quantachrome ChemBET 3000. The magnetic property of catalyst was

measured using a vibrating sample magnetometer (VSM, Magnetic Danesh Pajoh Inst). Inductively coupled plasma optical emission spectroscopy (ICP-OES) was carried out on a 76004555 SPECTRO ARCOS ICP-OES analyzer. All yields refer to isolated products after purification by thin layer chromatography/ or column chromatography. In addition, all of the products were known compounds and they were characterized by ^{1}H NMR, ^{13}C NMR spectroscopy, and mass spectrometry and comparison of their melting points with known compounds.

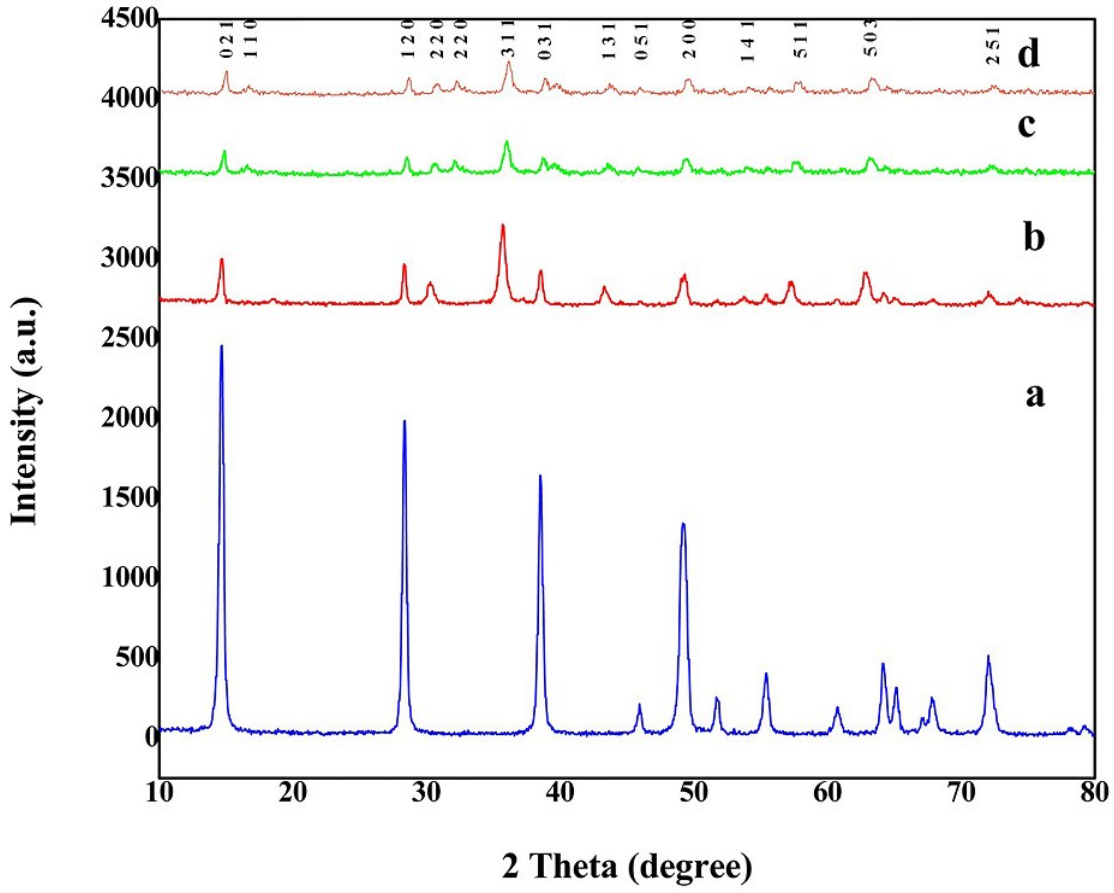

Fig. S1. XRD pattern of Boehmite NPs (a), Fe_3O_4@Boehmite NPs (b), Fe_3O_4@Boehmite-NH_2-Co^{II} NPs (c) and 7th reused Fe_3O_4@Boehmite- NH_2 -Co^{II} NPs (d).

Table 1. Specific surface area (S_{BET}), pore volume and mean pore diameter of Boehmite NPs (a), Fe_3O_4@Boehmite NPs (b) and Fe_3O_4@Boehmite-NH_2-Co^{II} NPs (c).

Samples	S_{BET} ($m^2\ g^{-1}$)	Total pore volume ($cm^3\ g^{-1}$)	Mean pore diameter (nm)
Boehmite NPs	20	0.32	36
Fe_3O_4@Boehmite NPs	46	0.13	28
Fe_3O_4@Boehmite-NH_2-Co^{II} NPs	34	0.40	34

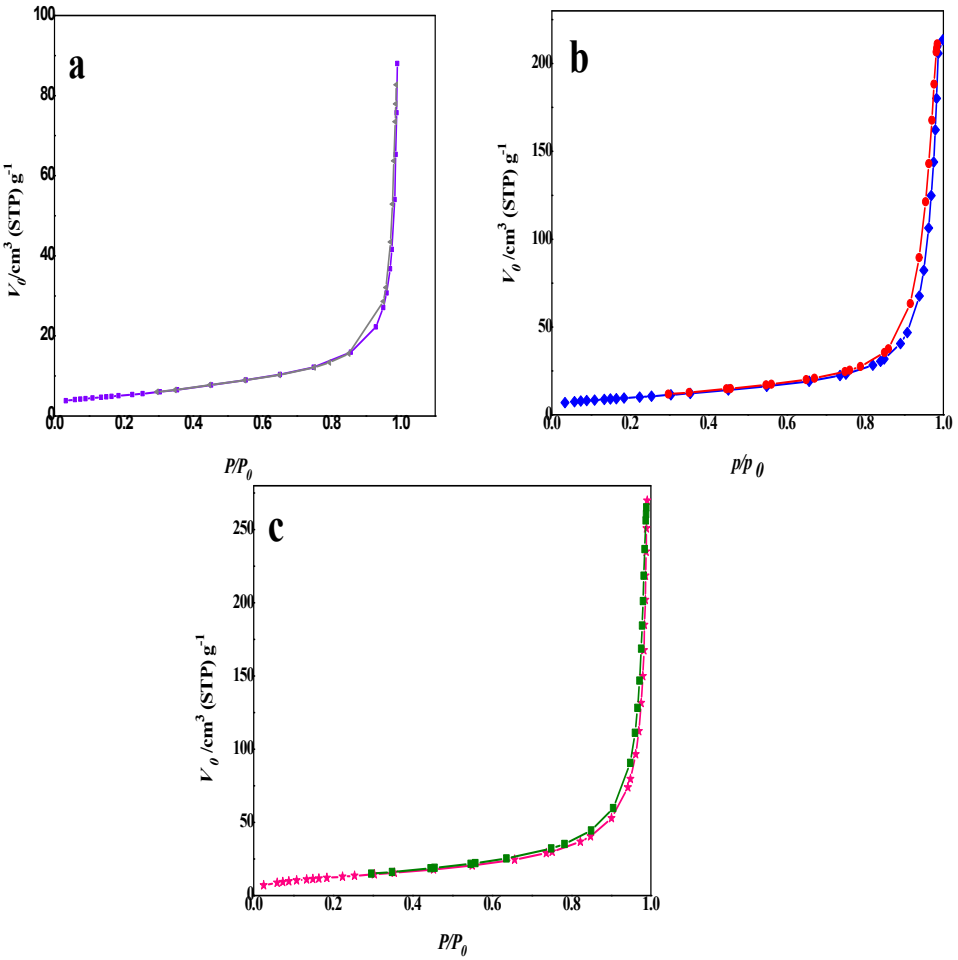

Fig. S2. The nitrogen adsorption-desorption isotherm of Boehmite NPs (a), Fe_3O_4@Boehmite NPs (b) and Fe_3O_4@Boehmite-NH_2-Co^{II} NPs (c).

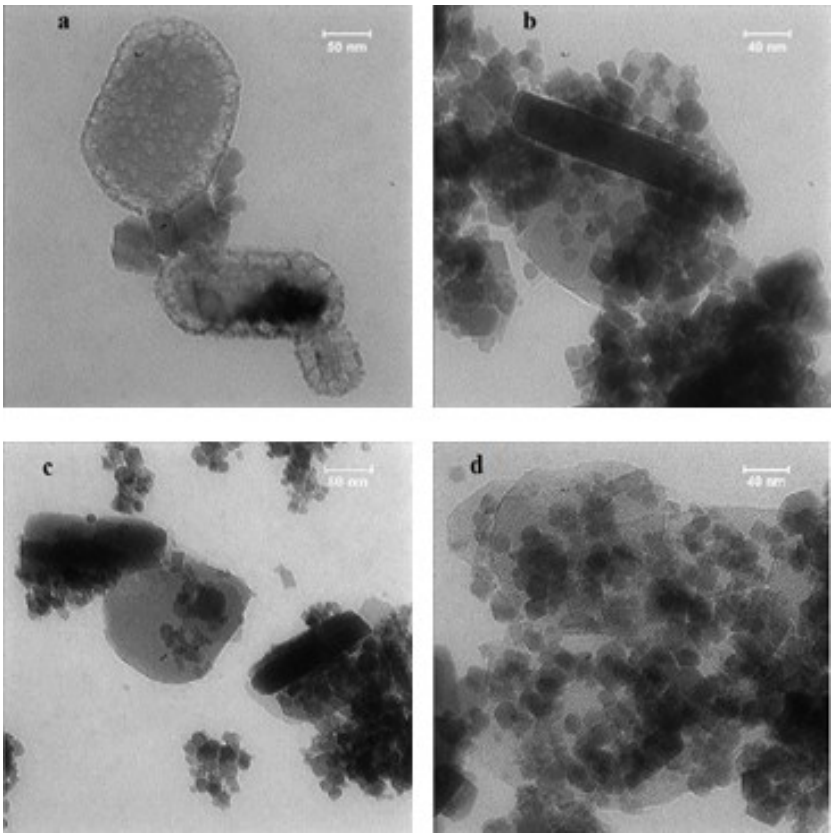

Fig. S3. TEM images of the fresh Fe_3O_4@Boehmite-NH_2-Co^{II} NPs (a and b) and 7th recovered Fe_3O_4@Boehmite-NH_2-Co^{II} NPs (c and d).

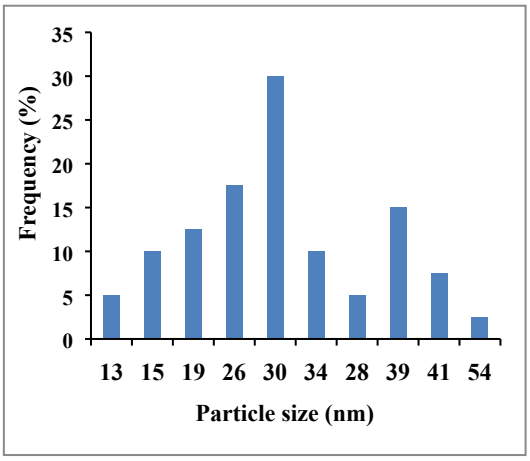

Fig. S4. Particle size distribution histogram of Fe_3O_4@Boehmite-NH_2-Co^{II} NPs.

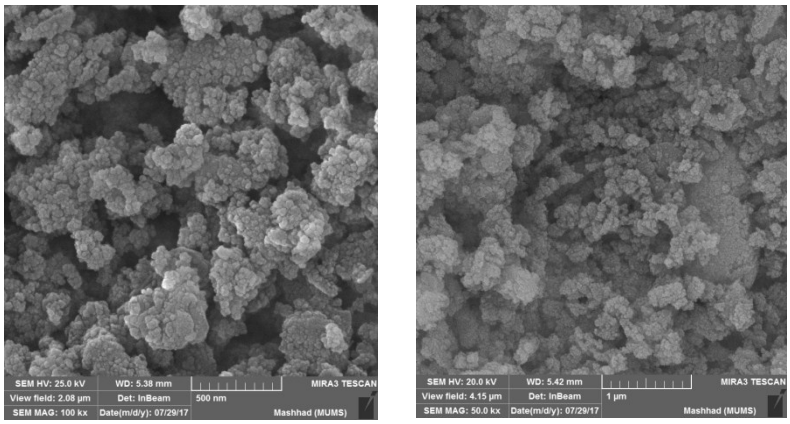

Fig. S5. FE-SEM images of Fe_3O_4@Boehmite-NH_2-Co^{II} NPs.

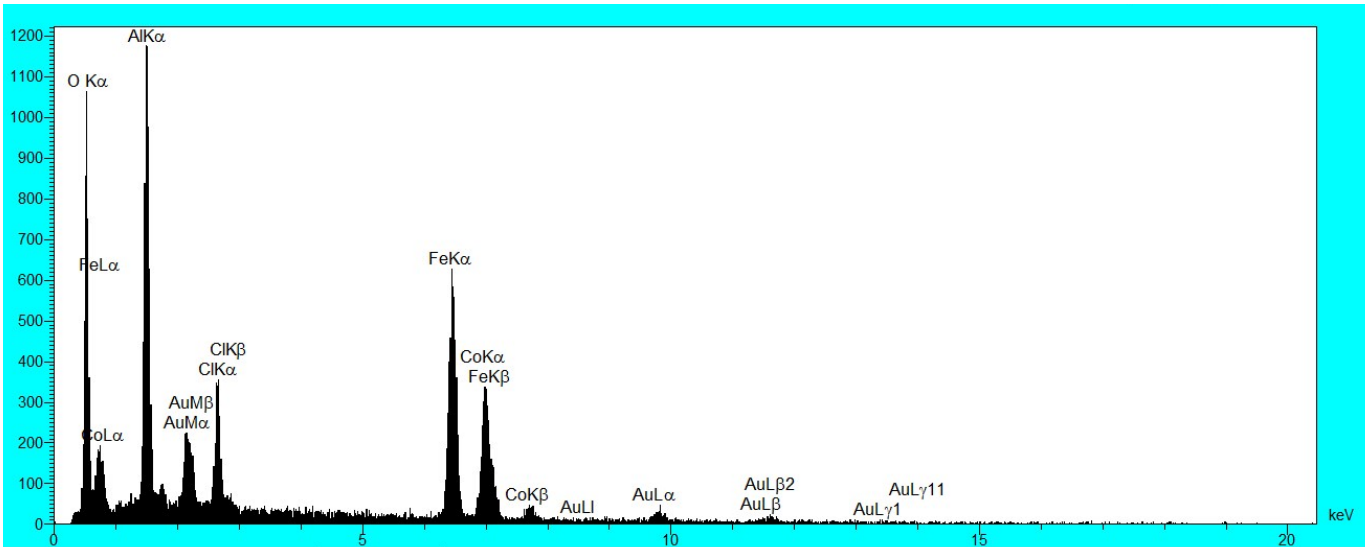

Fig. S6. EDX spectrum of Fe_3O_4@Boehmite-NH_2-Co^{II} NPs.

Table 2. Thermogravimetric analysis (TGA) and elemental analysis (EA) results.

Samples	Weight loss (%)	Organic grafted segments (mmol g^{-1})	Elemental analysis (%)	
			C	N
Fe_3O_4@Boehmite NPs	9	-	-	-
Fe_3O_4@Boehmite-Pr-Cl	18	1.16	4	-
Fe_3O_4@Boehmite-NH_2-Co^{II} NPs	33	1.03[a]	7.05	2.3

[a] triethylenetetramine

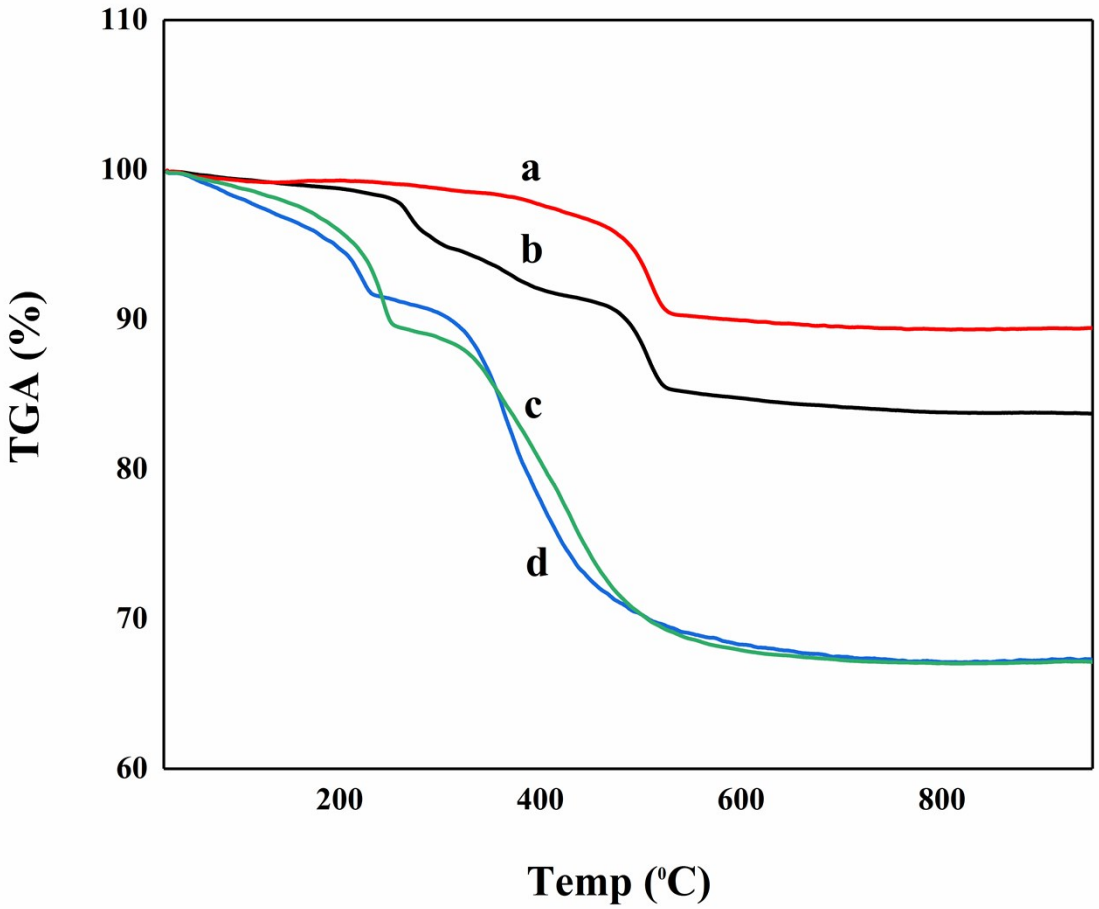

Fig. S7. TGA thermograms of Fe_3O_4@Boehmite NPs (a), Fe_3O_4@Boehmite-Pr-Cl (b), Fe_3O_4@Boehmite-NH_2-Co^{II} NPs (c) and 7th reused Fe_3O_4@Boehmite- NH_2 -Co^{II} NPs (d).

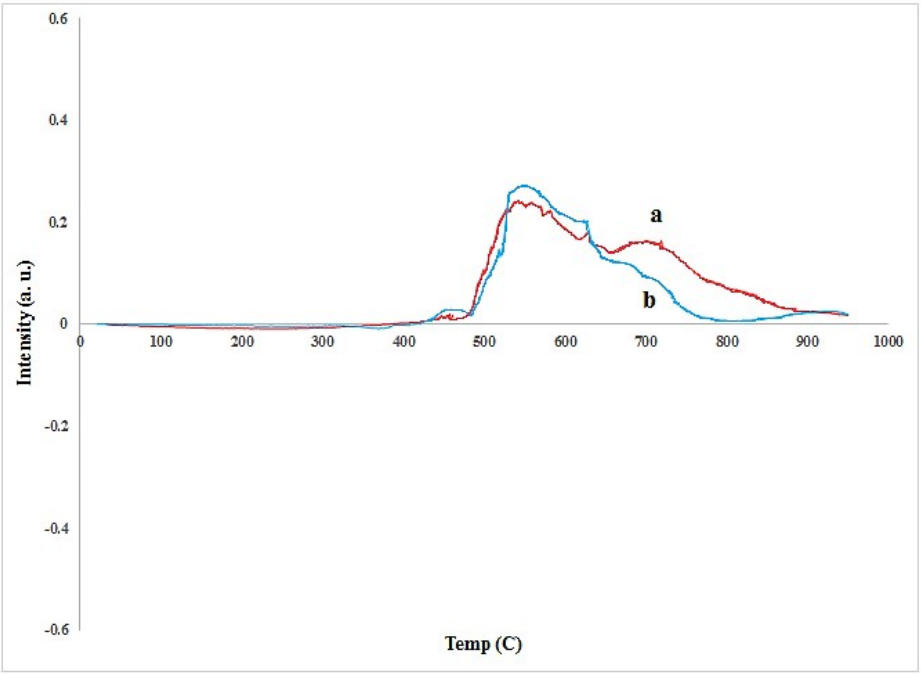

Fig. S8. H_2-TPR curves of Fe_3O_4@Boehmite-NH_2-Co^{II} NPs (a) and 7th reused Fe_3O_4@Boehmite- NH_2 -Co^{II} NPs (b).

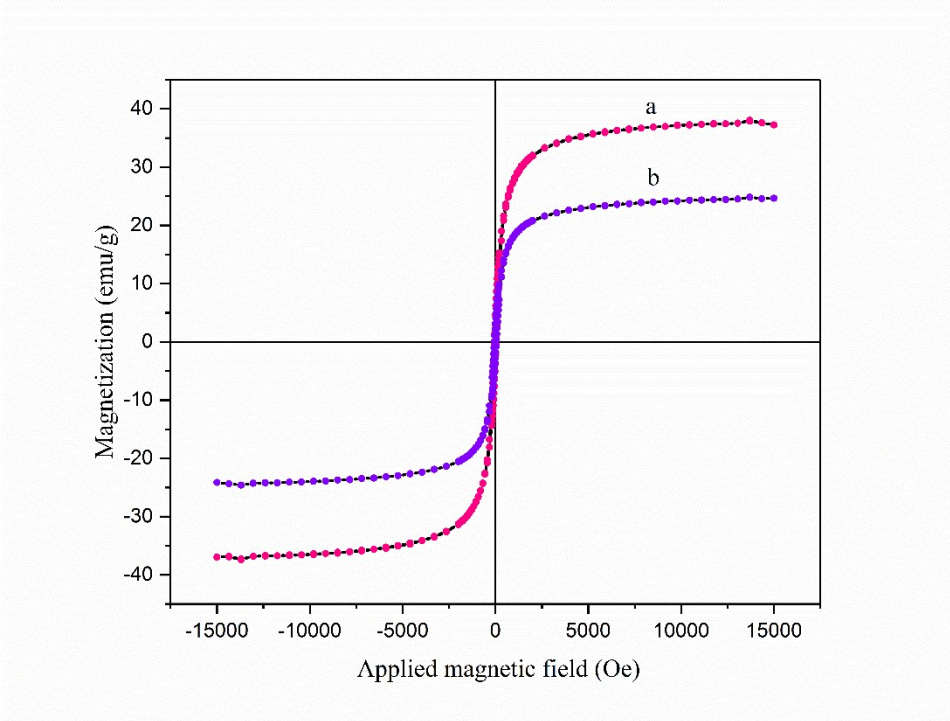

Fig. S9. Magnetization curves of Fe_3O_4@Boehmite NPs (a) and Fe_3O_4@Boehmite-NH_2-Co^{II} NPs (b).

Table 3. Optimization of reaction conditions for Suzuki–Miyaura coupling reaction.

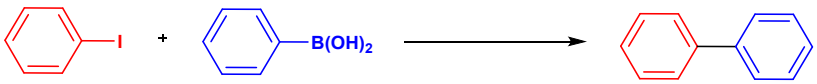

Entry	Catalyst (mol%)	Molar ratio of 4-Iodobenzene/Base	Base	Solvent	Temperature (°C)	Time (min)	Isolated Yield (%)
1	0.33	1/2	K_2CO_3	DMF	100	60	65
2	0.33	1/2	K_2CO_3	DMSO	100	60	60
3	0.33	1/2	K_2CO_3	PEG	100	60	60
4	0.33	1/2	K_2CO_3	THF	100	15 (h)	35
5	0.33	1/2	K_2CO_3	*n*-Hexane	100	20 (h)	20
6	0.33	1/2	K_2CO_3	Toluene	100	15 (h)	30
7	0.33	1/2	K_2CO_3	1,4-Dioxane	100	15 (h)	40
8	0.33	1/2	K_2CO_3	CH_3CN	100	13 (h)	50
9	0.33	1/2	K_2CO_3	EtOH	100	60	70
10	0.33	1/2	K_2CO_3	H_2O	100	60	90
11	0.33	-	-	H_2O	100	24 (h)	0
12	0.33	1/2	Li_2CO_3	H_2O	100	60	65
13	0.33	1/2	$NaHCO_3$	H_2O	100	60	70
14	0.33	1/2	K_3PO_4	H_2O	100	60	75
15	0.33	1/2	KOH	H_2O	100	60	90
16	0.33	1/3	KOH	H_2O	100	30	98
17	0.33	1/4	KOH	H_2O	100	30	98
18	0.33	1/3	KOH	H_2O	90	30	95
19	**0.33**	**1/3**	**KOH**	**H_2O**	**80**	**30**	**95**
20	0.33	1/3	KOH	H_2O	70	45	87
21	0.33	1/3	KOH	H_2O	R.T	5 (h)	-
22	0.44	1/3	KOH	H_2O	80	30	95
23	0.22	1/3	KOH	H_2O	80	30	80
24	-	1/3	KOH	H_2O	80	24 (h)	20
25	0.003 (g)[a]	1/3	KOH	H_2O	80	24 (h)	20

26	0.003(g)[b]	1/3	KOH	H_2O	80	24 (h)	5
27	0.003(g)[c]	1/3	KOH	H_2O	80	24 (h)	5
28	0.003(g)[d]	1/3	KOH	H_2O	80	24 (h)	5
29	0.33[e]	1/3	KOH	H_2O	80	24 (h)	40

[a] Reaction was performed in the presence of Fe_3O_4NPs. [b] Reaction was performed in the presence of Fe_3O_4@Boehmite NPs. [c]Reaction was performed in the presence of Fe_3O_4@Boehmite-Pr-Cl . [d] Reaction was performed in the presence of Fe_3O_4@Boehmite-NH_2. [e]Reaction was performed in the presence of $CoCl_2.6H_2O$.

Table 4. Optimization of reaction conditions for Heck–Mizoroki cross coupling reaction.

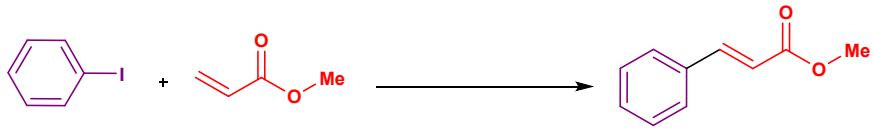

Entry	Catalyst (mol%)	Molar ratio of 4-Iodobenzene/Base	Base	Solvent	Temperature (°C)	Time (min)	Isolated Yield (%)
1	0.33	1/2	K_2CO_3	DMF	100	80	65
2	0.33	1/2	K_2CO_3	DMSO	100	80	65
3	0.33	1/2	K_2CO_3	PEG	100	70	60
4	0.33	1/2	K_2CO_3	THF	100	11(h)	40
5	0.33	1/2	K_2CO_3	*n*-hexane	100	17(h)	25
6	0.33	1/2	K_2CO_3	Toluene	100	17(h)	30
7	0.33	1/2	K_2CO_3	1,4-dioxane	100	13(h)	50
8	0.33	1/2	K_2CO_3	CH_3CN	100	11(h)	45
9	0.33	1/2	K_2CO_3	EtOH	100	90	65
10	0.33	1/2	K_2CO_3	H_2O	100	80	80
11	0.33	1/2	Li_2CO_3	H_2O	100	80	60
12	0.33	1/2	$NaHCO_3$	H_2O	100	80	70
13	0.33	1/2	KOH	H_2O	100	75	60
14	0.33	1/2	K_3PO_4	H_2O	100	70	85
15	0.33	-	-	H_2O	100	24 (h)	-
16	0.33	1/3	K_3PO_4	H_2O	100	75	92
17	0.33	1/4	K_3PO_4	H_2O	100	45	97

18	0.33	1/5	K_3PO_4	H_2O	100	45	97
19	0.33	1/4	K_3PO_4	H_2O	90	45	94
20	0.33	1/4	K_3PO_4	H_2O	80	45	94
21	0.33	1/4	K_3PO_4	H_2O	70	45	83
22	0.33	1/4	K_3PO_4	H_2O	R.T	5 (h)	-
23	**0.44**	**1/4**	**K_3PO_4**	**H_2O**	**80**	**45**	**95**
24	0.55	1/4	K_3PO_4	H_2O	80	45	95
25	-	1/4	K_3PO_4	H_2O	80	24 (h)	20
26	0.004 (g)[a]	1/4	K_3PO_4	H_2O	80	24 (h)	15
27	0.004 (g)[b]	1/4	K_3PO_4	H_2O	80	24 (h)	Trace
28	0.004 (g)[c]	1/4	K_3PO_4	H_2O	80	24 (h)	Trace
29	0.004 (g)[d]	1/4	K_3PO_4	H_2O	80	24 (h)	Trace
30	0.44[e]	1/4	K_3PO_4	H_2O	80	24 (h)	35

[a] Reaction was performed in the presence of Fe_3O_4NPs. [b] Reaction was performed in the presence of Fe_3O_4@Boehmite NPs. [c] Reaction was performed in the presence of Fe_3O_4@Boehmite-Pr-Cl. [d] Reaction was performed in the presence of Fe_3O_4@Boehmite-NH_2. [e] Reaction was performed in the presence of $CoCl_2 .6H_2O$.

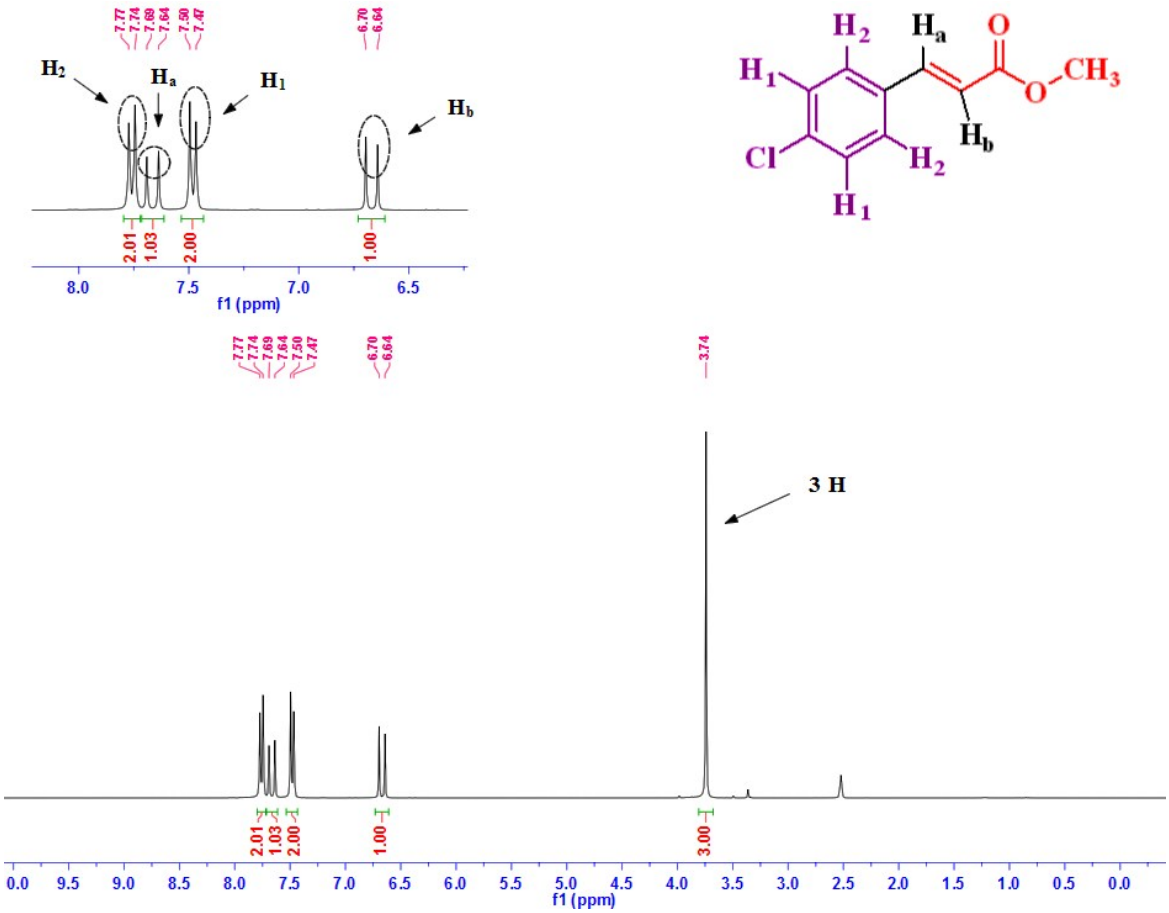

Fig. S10. ^{1}H NMR (300 MHz, $CDCl_3$) of methyl 3-(4-chlorophenyl)acrylate (2c).

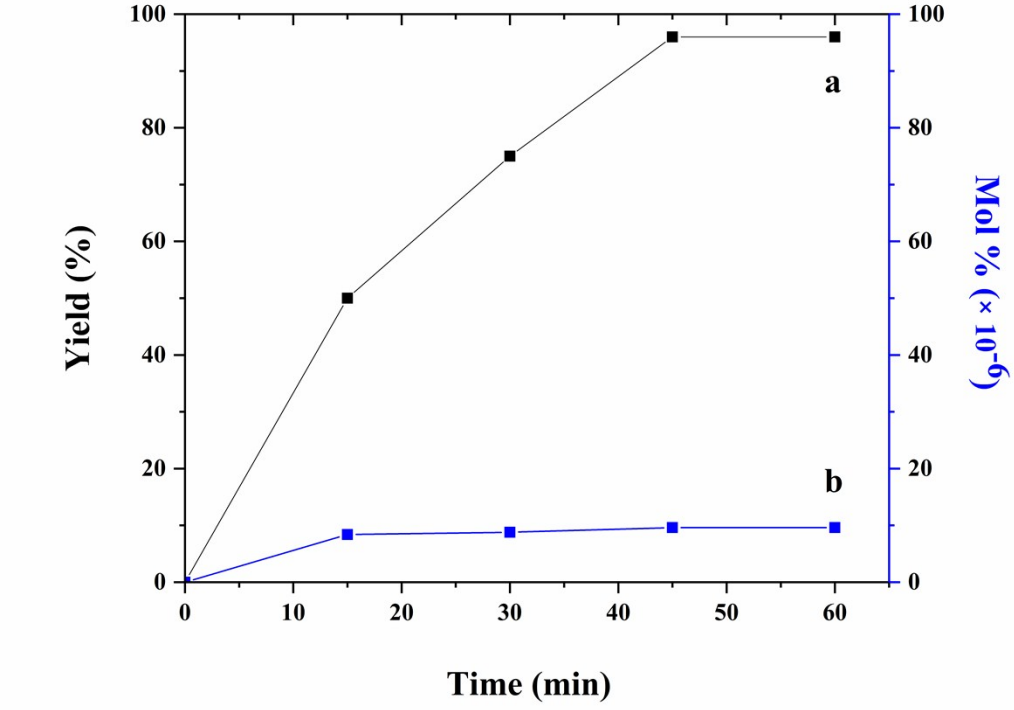

Fig. S11. Time-dependent correlation of the yield (a) and cobalt leaching (b) in model reaction.

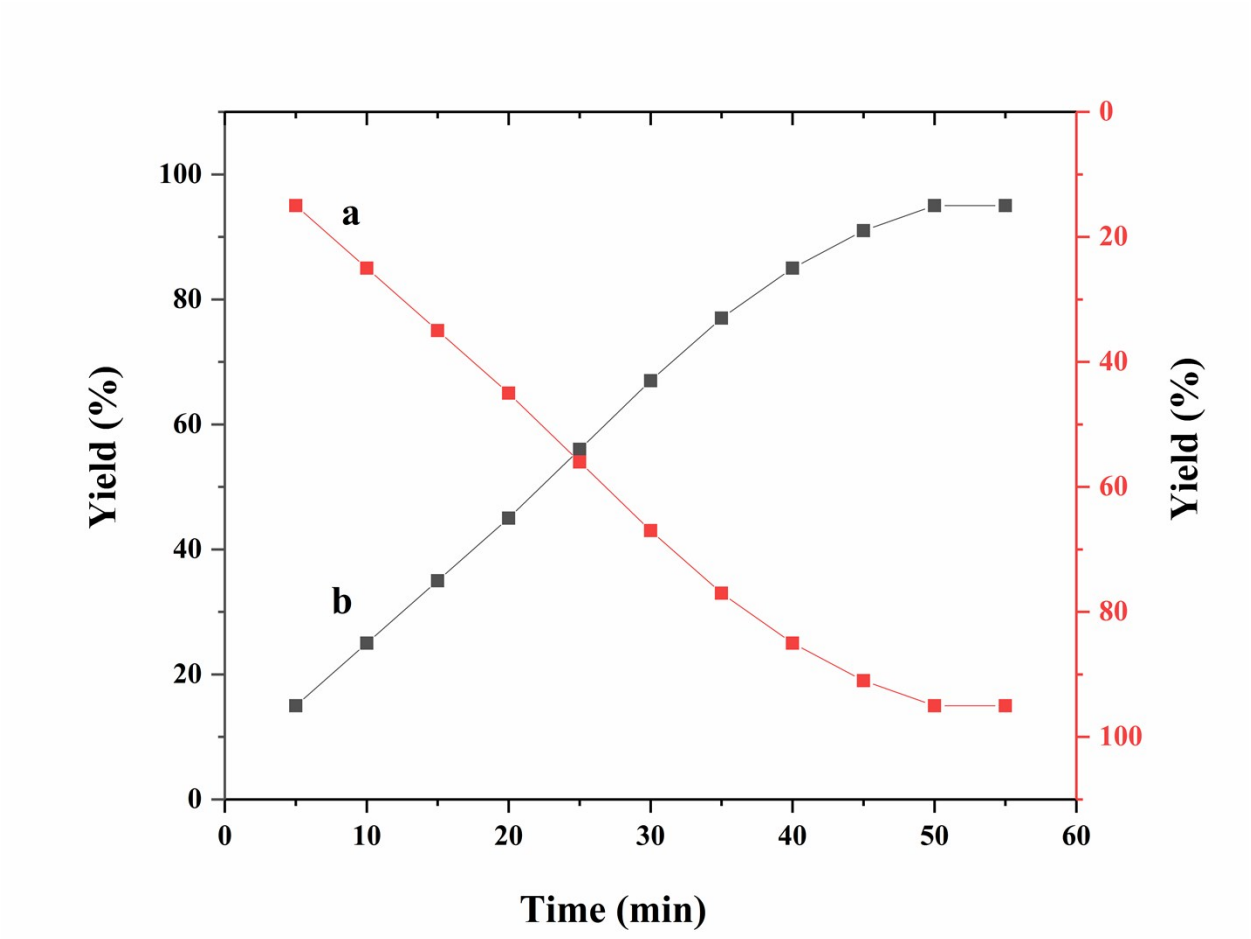

Fig. S12. Time-dependent correlation of the yield of Heck-Mizoroki cross coupling reaction in the absence (a) and in the presence (b) of Boehmite-NH_2 NPs.

1, 1'-Biphenyl (1a): [1] Mp 70-72 ˚C (Lit. 70-71˚C); ^{1}H NMR (400 MHz, $CDCl_3$): δ 7.55 (d , J = 8.2 Hz, 4H), 7.39 (t, J = 7.6 Hz, 4H), 7.31-7.27 (m, 2H); ^{13}C NMR (125 MHz, $CDCl_3$) δ 141.25, 128.75, 127.24, 127.17; MS, *m/z* (%): 154 [M^+].

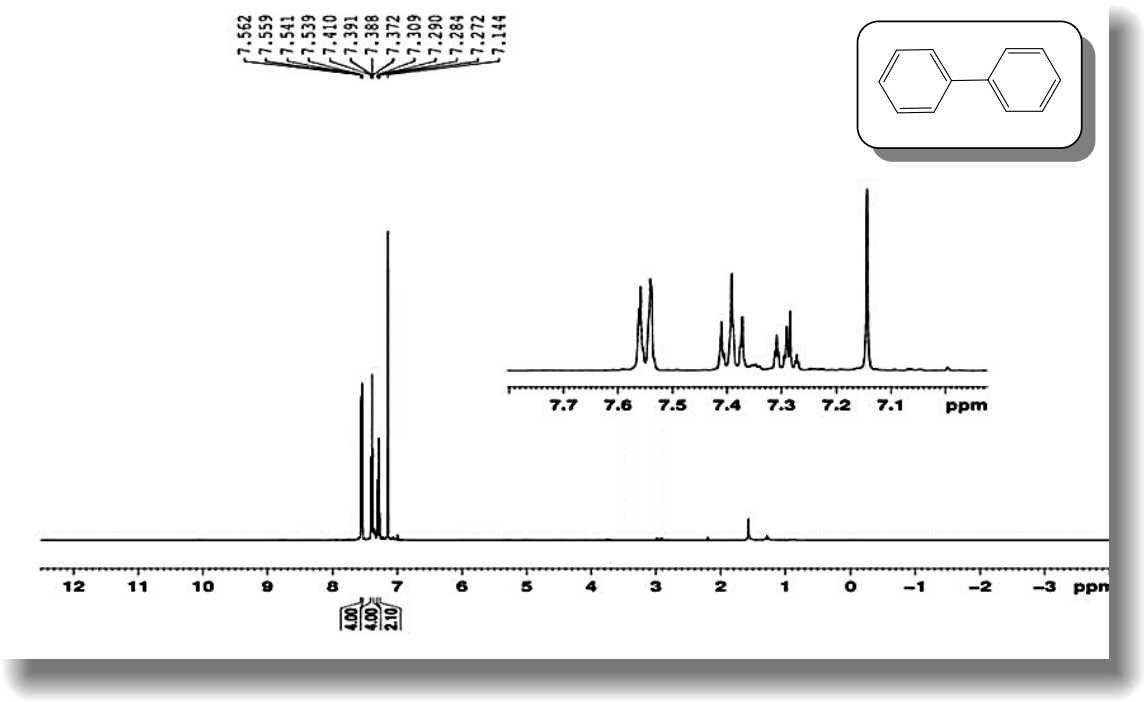

Figure 1-A: ^{1}H NMR (400 MHz, $CDCl_3$) of 1, 1'-Biphenyl (1a).

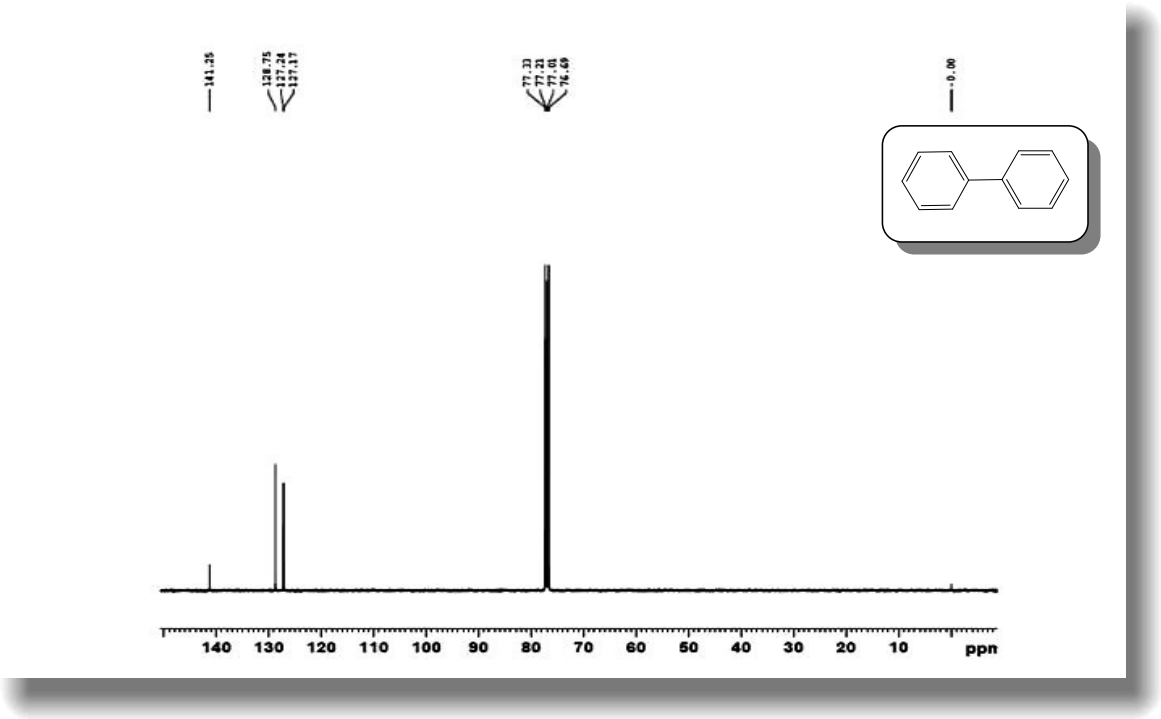

Figure 1-B: ^{13}C NMR (125 MHz, $CDCl_3$) of 1, 1'-Biphenyl (1a).

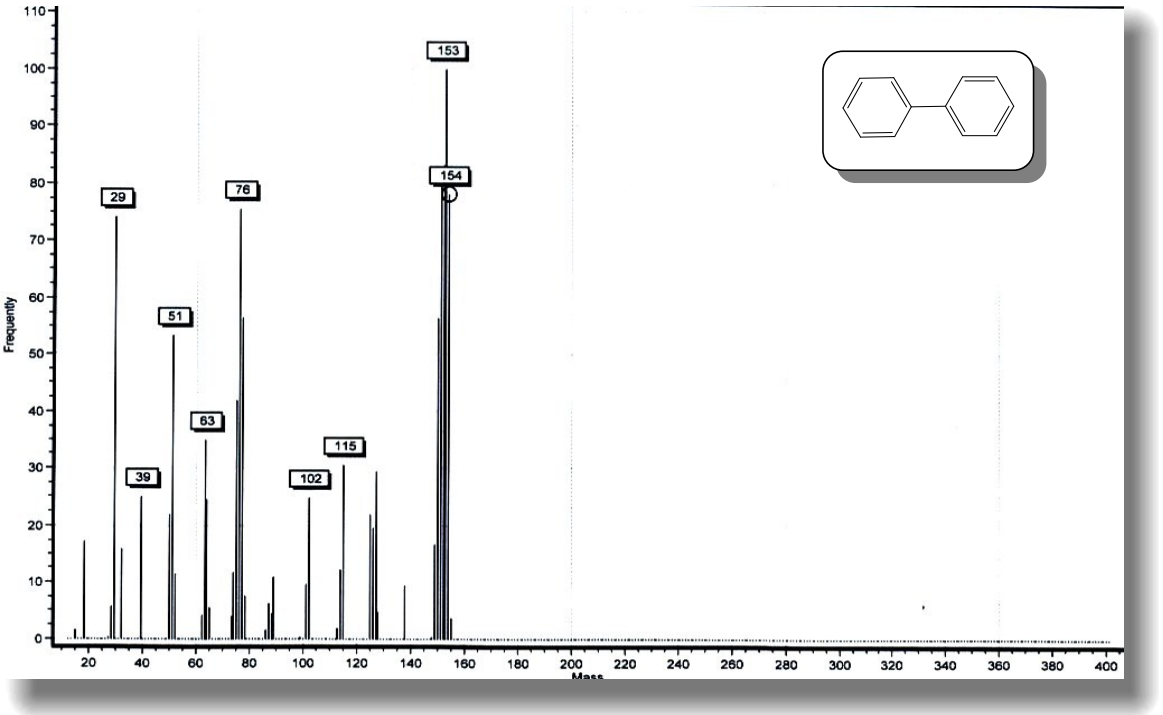

Figure 1-C: Mass spectrum of 1, 1'-Biphenyl (1a).

4-Nitro-1, 1'-biphenyl (1b):[2] Mp 107-109 ˚C (Lit. 108-109 ˚C);^{1}H NMR (400 MHz, $CDCl_3$) δ 8.33 (d, *J* = 8.8 Hz, 2H), 7.67-7.65 (d, *J* = 8.4 Hz, 2H), 7.78-7.76 (d, *J* = 8.8 Hz, 2H), 7.55-7.46 (m, 3H); ^{13}C NMR (125 MHz, $CDCl_3$) δ 147.18, 146.65, 138.32, 128.72, 128.49, 127.35, 126.95, 123.66; MS, *m/z* (%): 199 [M^+].

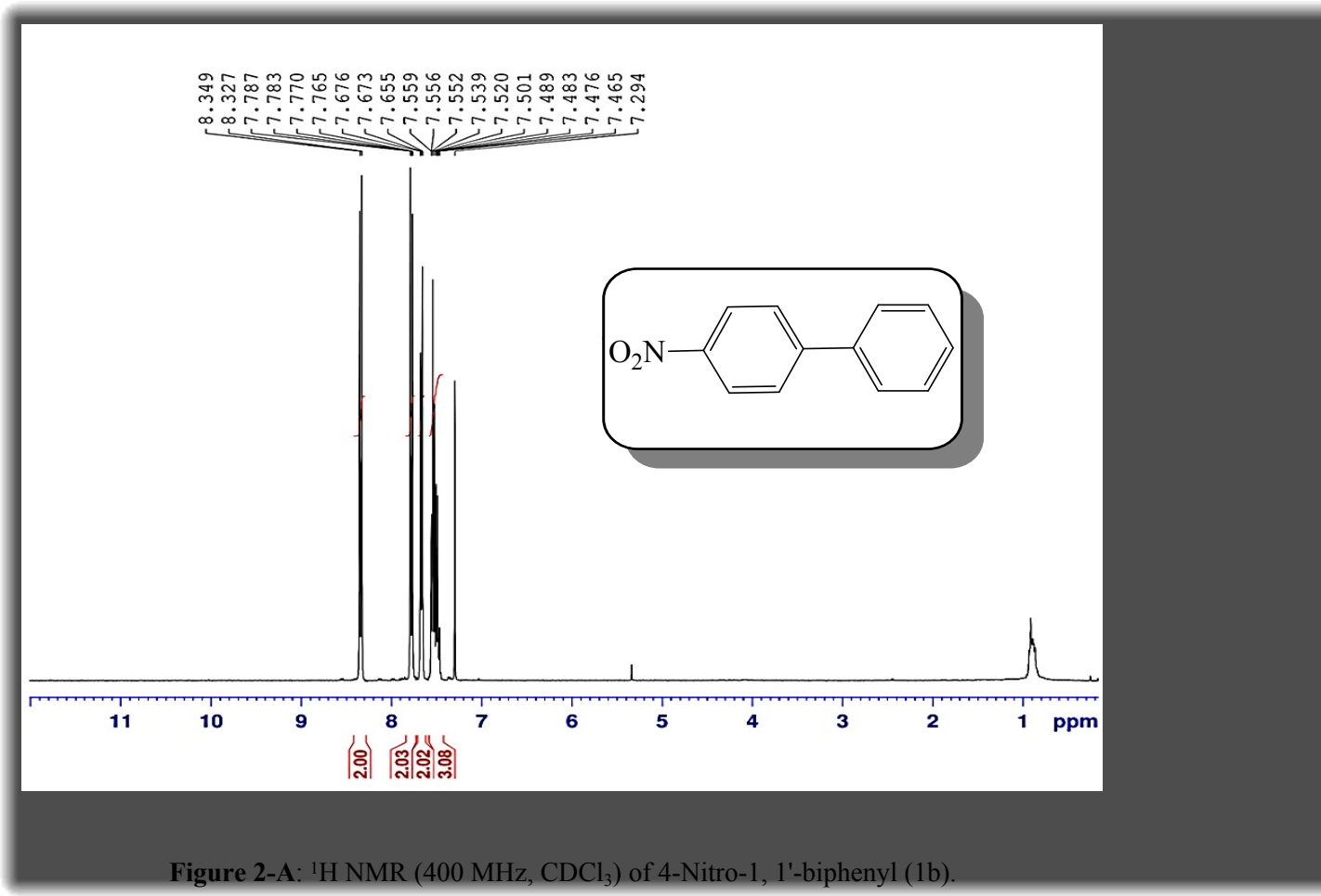

Figure 2-A: ^{1}H NMR (400 MHz, $CDCl_3$) of 4-Nitro-1, 1'-biphenyl (1b).

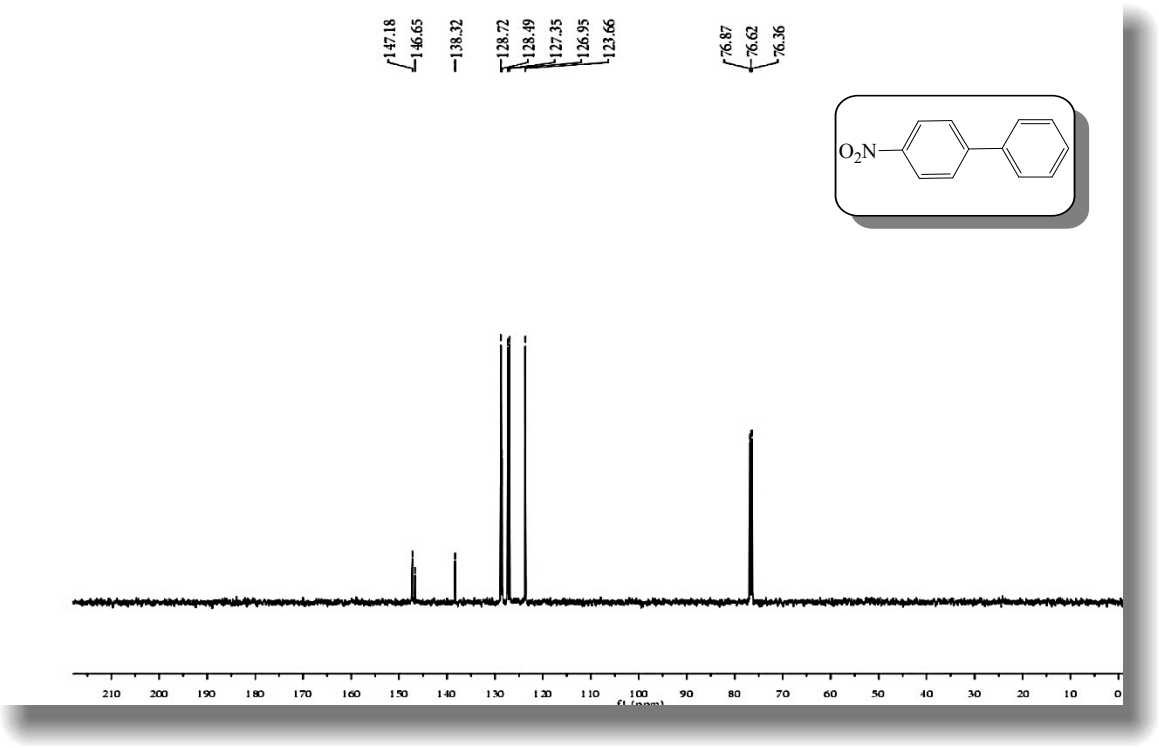

Figure 2-B: ^{13}C NMR (125 MHz, $CDCl_3$) of 4-Nitro-1, 1'-biphenyl (1b).

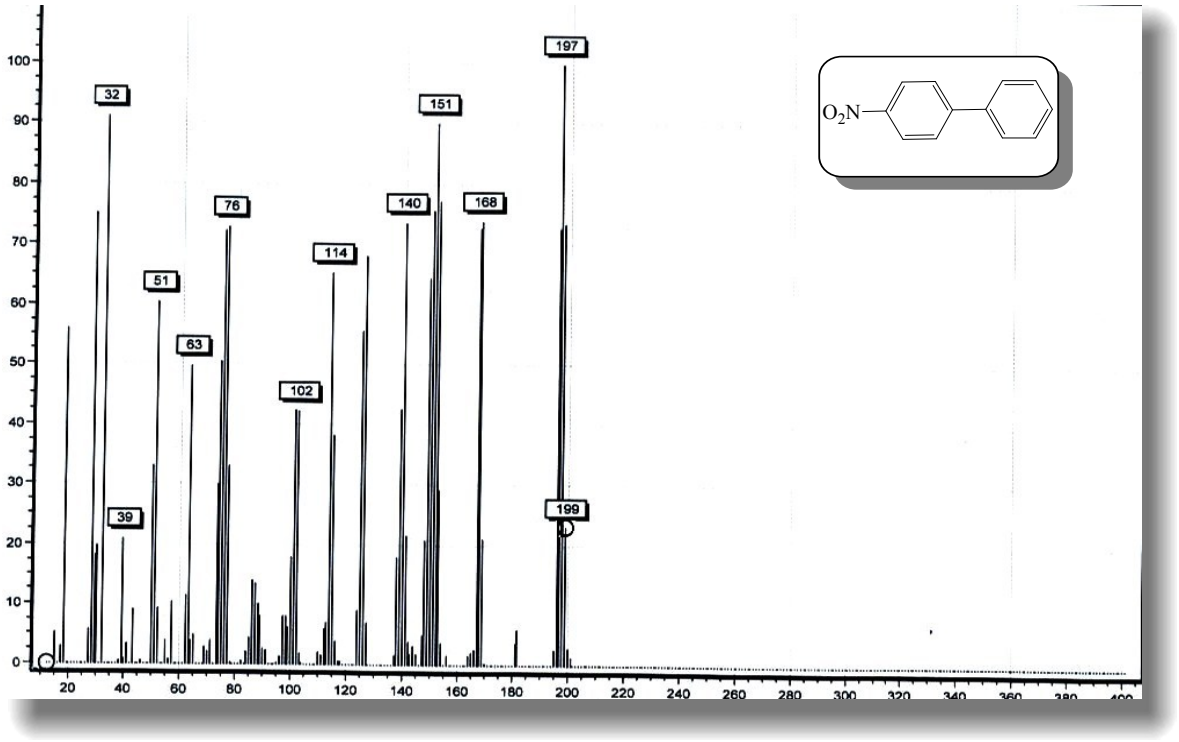

Figure 2-C: Mass spectrum of 4-Nitro-1, 1'-biphenyl (1b).

4-Chloro-1, 1'-biphenyl (1c): [3] Mp 71-73 ˚C (Lit. 71-73˚C); MS, *m/z* (%): 189 [M^+].

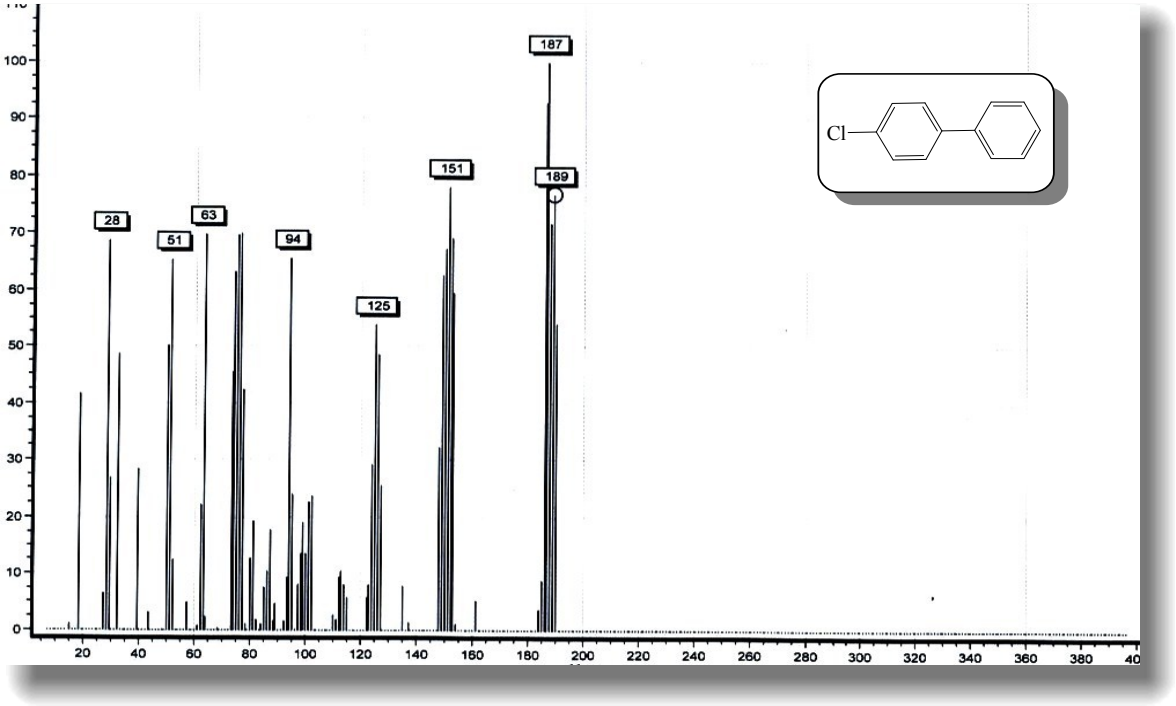

Figure 3-C: Mass spectrum of 4-Chloro-1, 1'-biphenyl (1c).

4-Methoxy-1, 1'-biphenyl (1d): [4] Mp 87-90 ˚C (Lit. 89-91˚C); ^{1}NMR (400 MHz, $CDCl_3$) δ 7.45 (t, J = 8.4 Hz, 4H), 7.34 (t, J = 7.6 Hz, 2H), 7.21 (t, J = 6.8 Hz, 1H), 6.89 (d, J = 8.8 Hz, 2H), 3.75 (s, 3H); ^{13}C NMR (125 MHz, $CDCl_3$) δ 159.17, 140.88, 133.82, 128.72, 128.16, 126.75, 114.23, 55.36; MS, *m/z* (%): 184 [M^+].

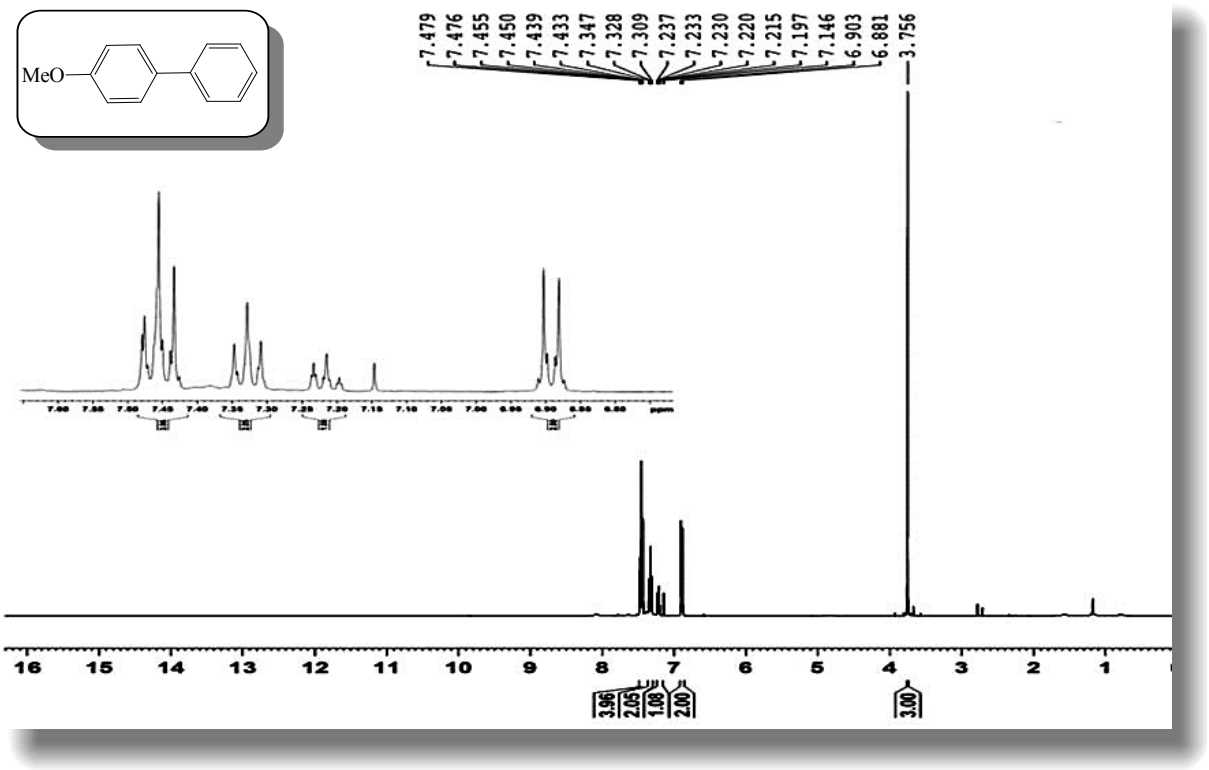

Figure 4-A: ^{1}H NMR (400 MHz, $CDCl_3$) of 4-Methoxy-1, 1'-biphenyl (1d).

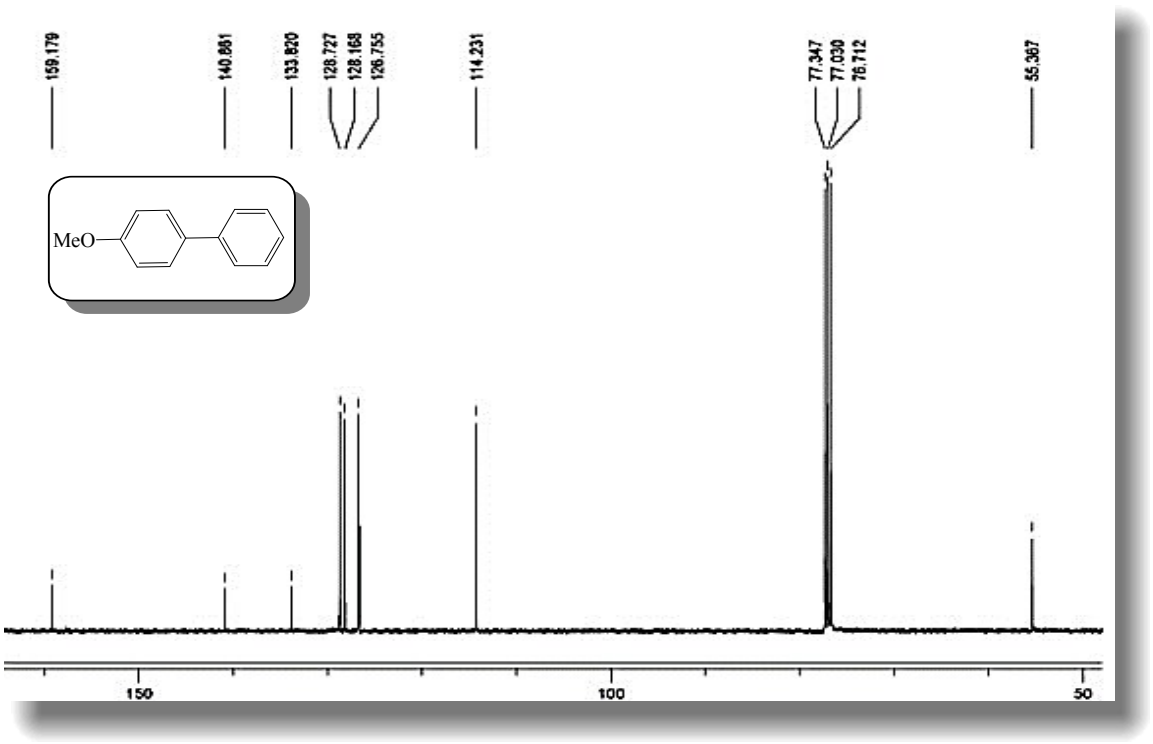

Figure 4-B: ^{13}C NMR (125 MHz, $CDCl_3$) of 4-Methoxy-1, 1'-biphenyl (1d).

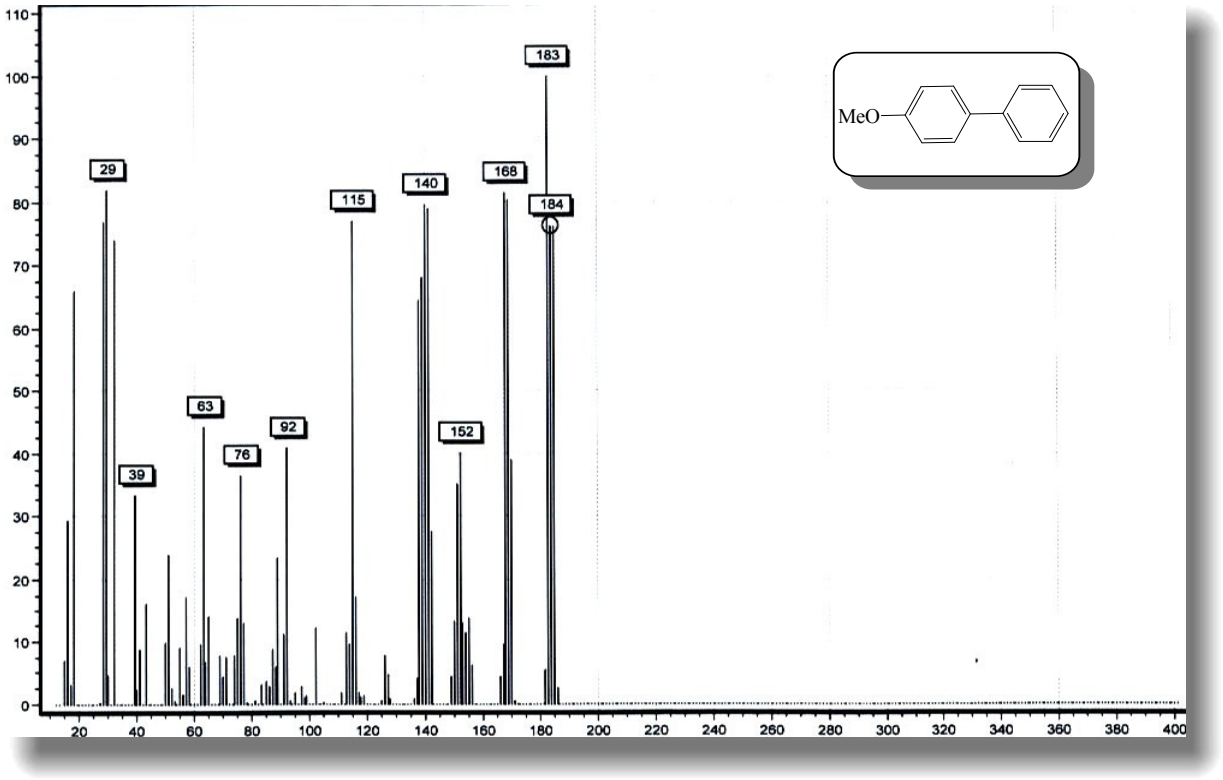

Figure 4-C: Mass spectrum of 4-Methoxy-1, 1'-biphenyl (1d).

4-Methyl-1, 1'-biphenyl (1e): [5] Mp 43-44 ˚C (Lit. 45-47˚C); ^{1}H NMR (400 MHz, $CDCl_3$): δ 7.64 (d, *J* = 8.0 Hz, 2H), 7.54 (d, *J* = 8.0 Hz, 2H), 7.47 (t, *J* = 7.2 Hz, 2H), 7.37 (t, *J* = 7.2 Hz, 1H), 7.28 (d, *J* = 8.0 Hz, 2H), 2.44 (s, 3H) ppm; ^{13}C NMR (125 MHz, $CDCl_3$) δ 141.69, 138.89, 137.56, 130.02, 129.26, 127.71, 127.54, 127.52, 21.65 ppm.

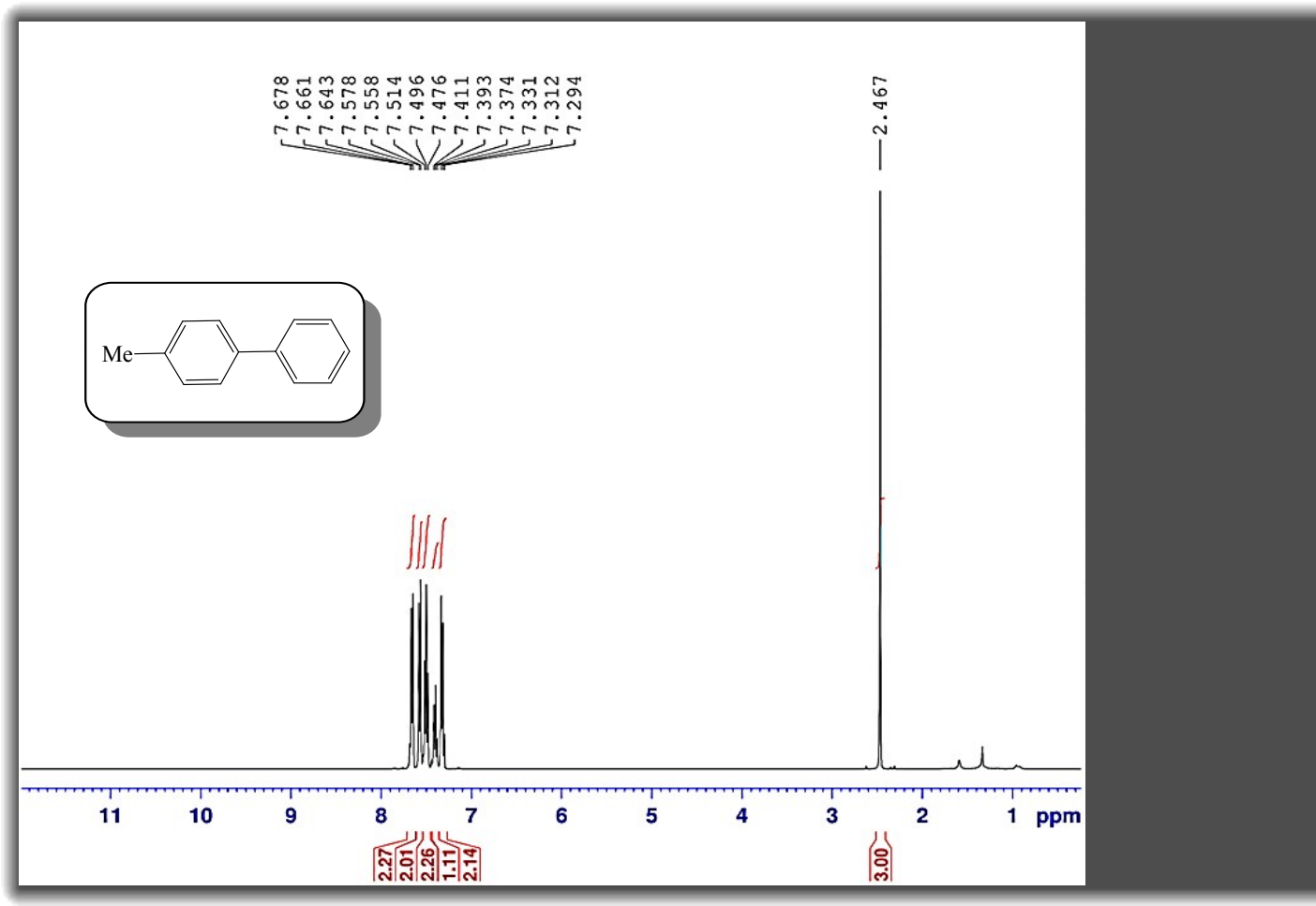

Figure 5-A: ^{1}H NMR (400 MHz, $CDCl_3$) of 4-Methyl-1, 1'-biphenyl (1e).

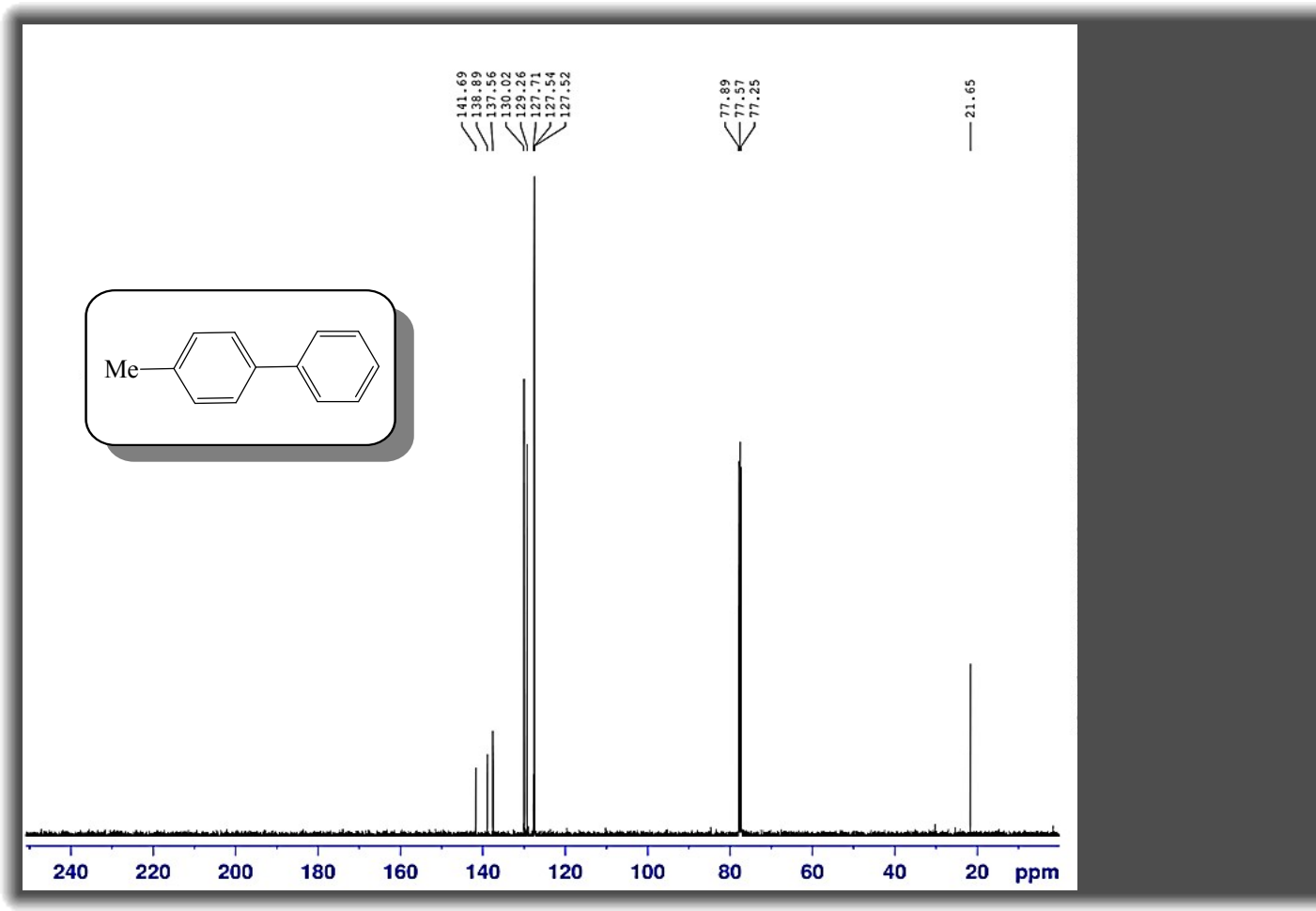

Figure 5-B: ^{13}C NMR (125 MHz, $CDCl_3$) of 4-Methyl-1, 1'-biphenyl (1e).

3-Methyl-4-phenylnitrobenzene (1f): [6] Mp 53-55 ˚C (Lit. 53-55 ˚C)**;** MS, *m/z* (%): 213 [M^+].

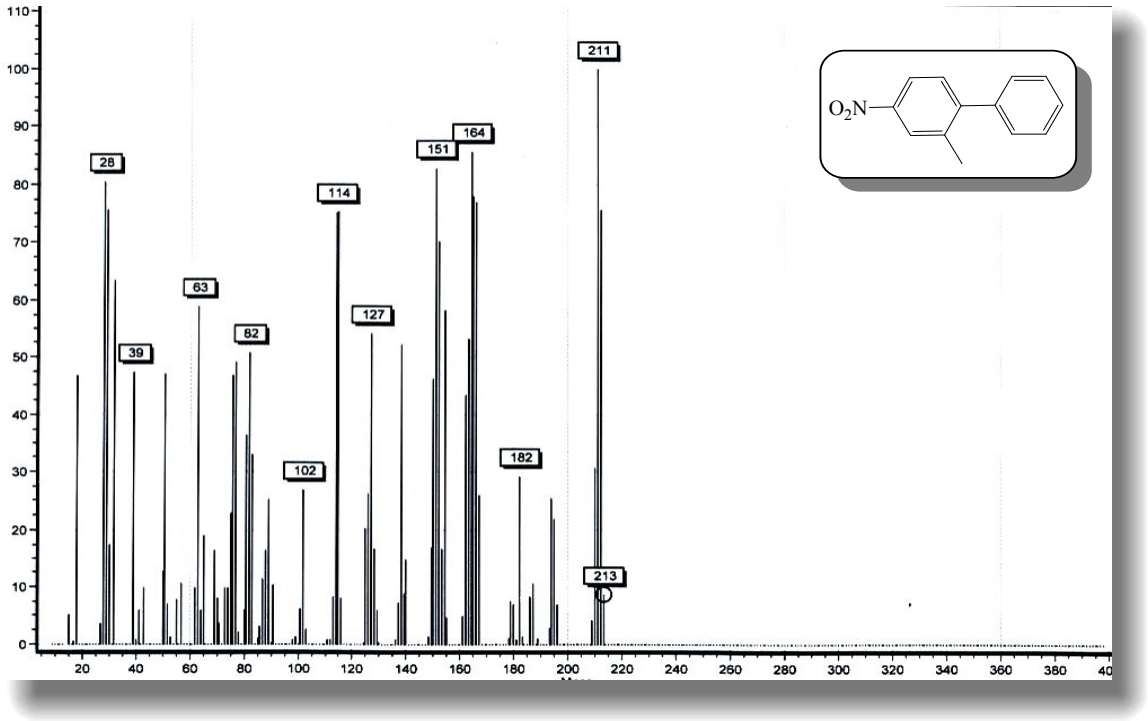

Figure 6-C: Mass spectrum of 2-Methyl-4-nitro-1, 1'-biphenyl (1f).

2-Phenylthiophene (1g): [7] Mp 34-36 ˚C (Lit. 34-36˚C); ^{1}H NMR (300 MHz, $CDCl_3$) δ 7.59-7.62 (m, 2H), 7.06-7.38 (m, 6H).

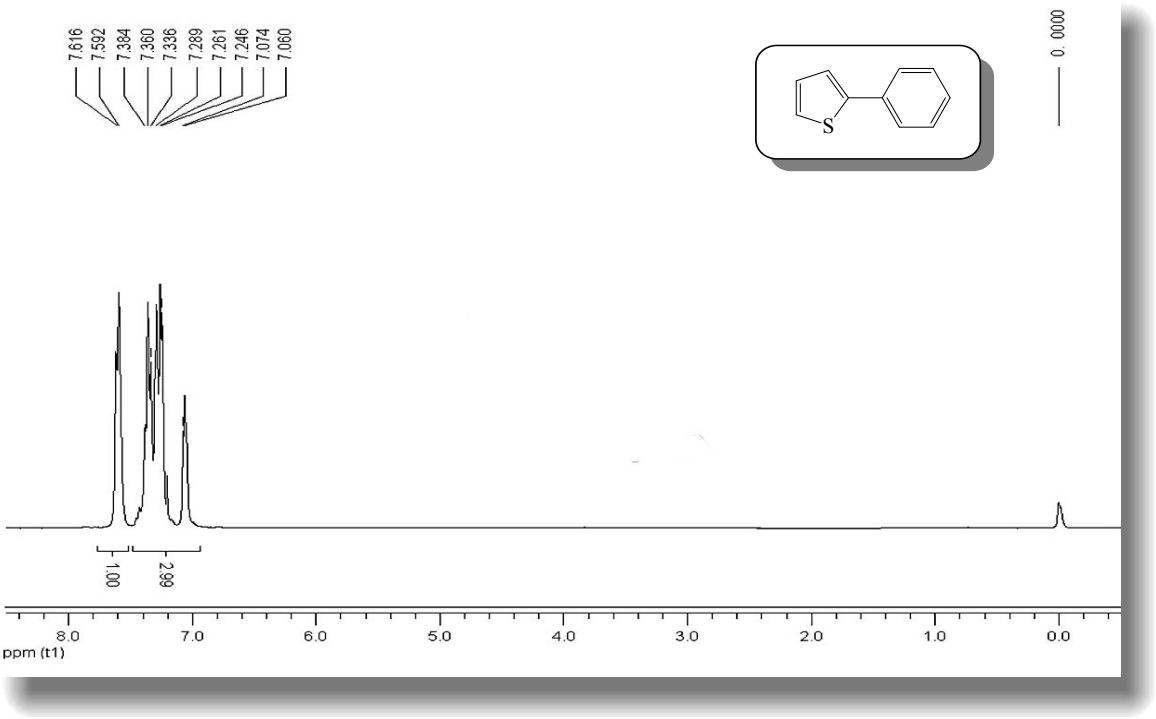

Figure 7-A: ^{1}H NMR (300 MHz, $CDCl_3$) of 2-Phenylthiophene (1g).

4-Cyano-1, 1'-biphenyl (1j): [8] Mp 85-87 ˚C (Lit. 84-86 ˚C); ^{1}H NMR (400 MHz, $CDCl_3$) δ 7.70-7.77 (q, 4H), 7.62 (d, 2H, *J* = 7.2 Hz), 7.46-7.54 (m, 3H); ^{13}C NMR (125 MHz, $CDCl_3$) δ 145.68, 139.19, 132.60, 129.11, 128.66, 127.74, 127.23, 118.94, 110.93; MS, *m/z* (%): 179 [M^+].

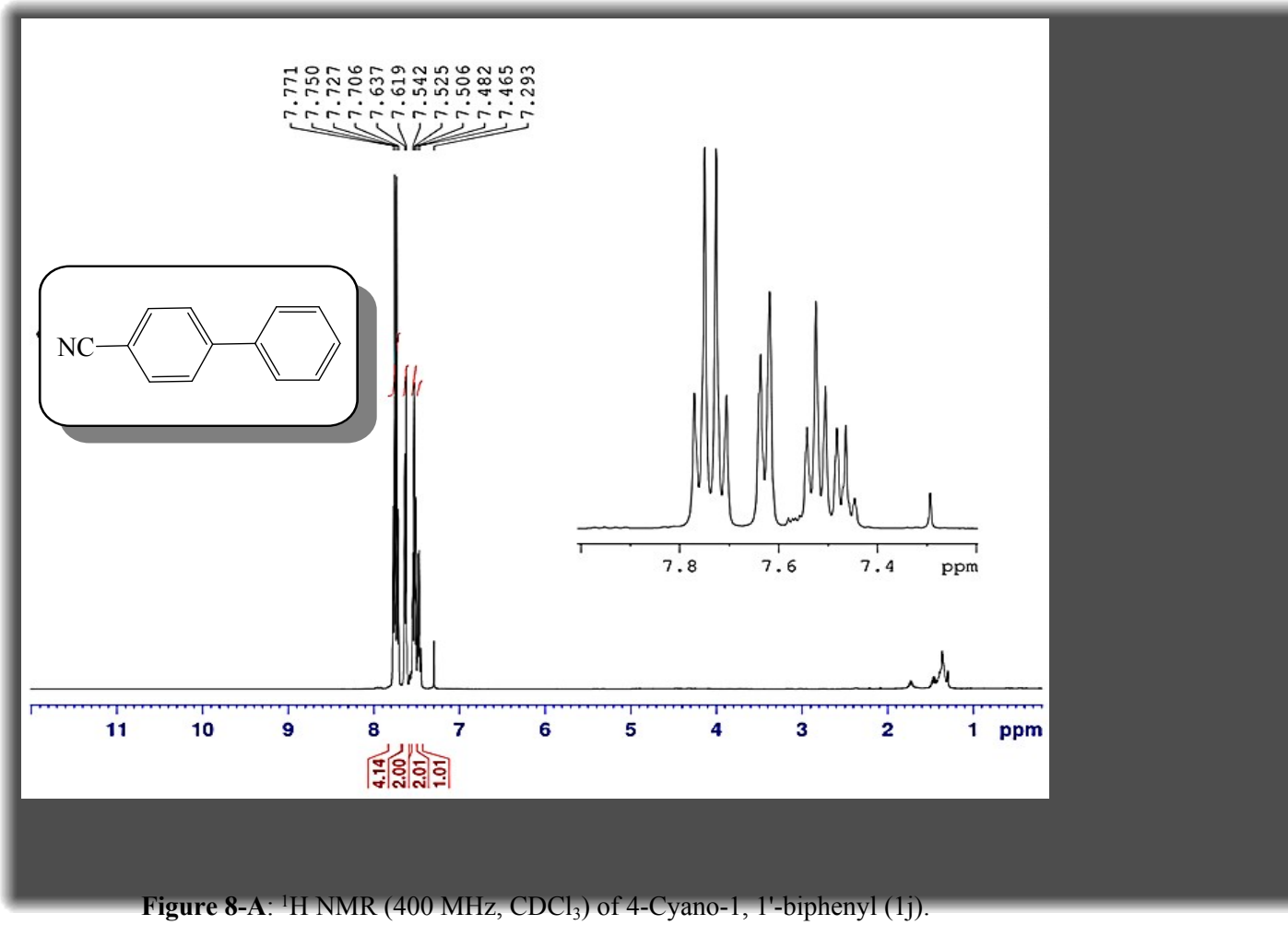

Figure 8-A: ^{1}H NMR (400 MHz, $CDCl_3$) of 4-Cyano-1, 1'-biphenyl (1j).

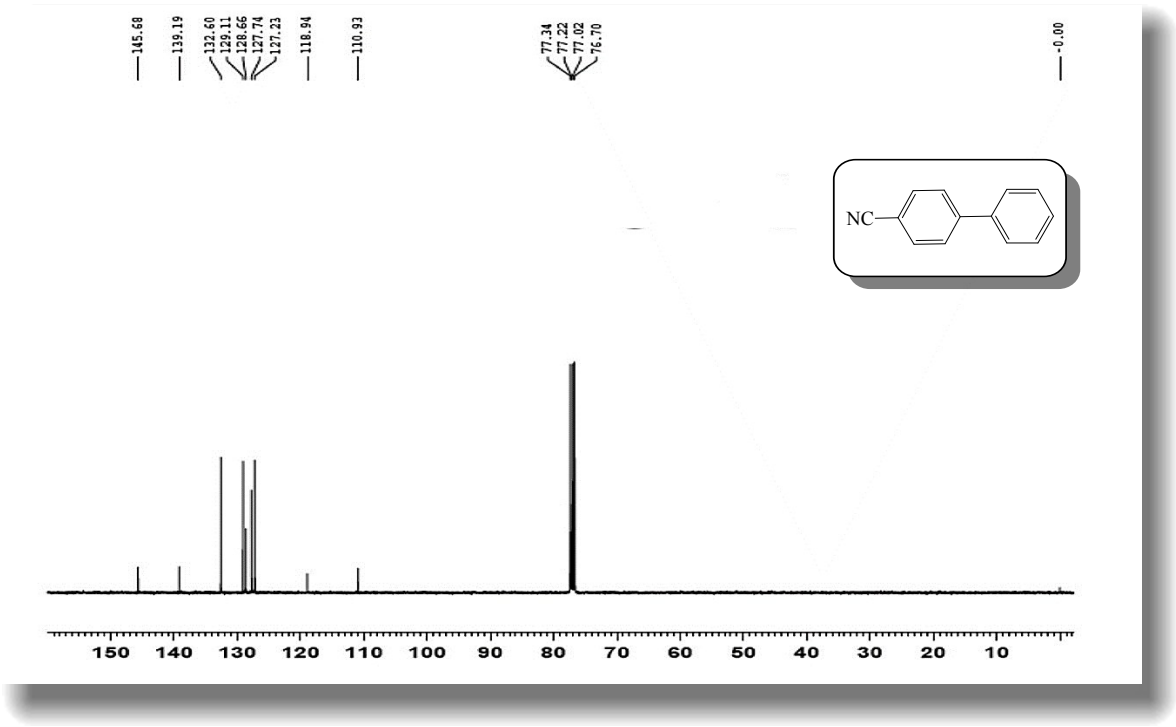

Figure 8-B: ^{13}C NMR (125 MHz, $CDCl_3$) of 4-Cyano-1, 1'-biphenyl (1j).

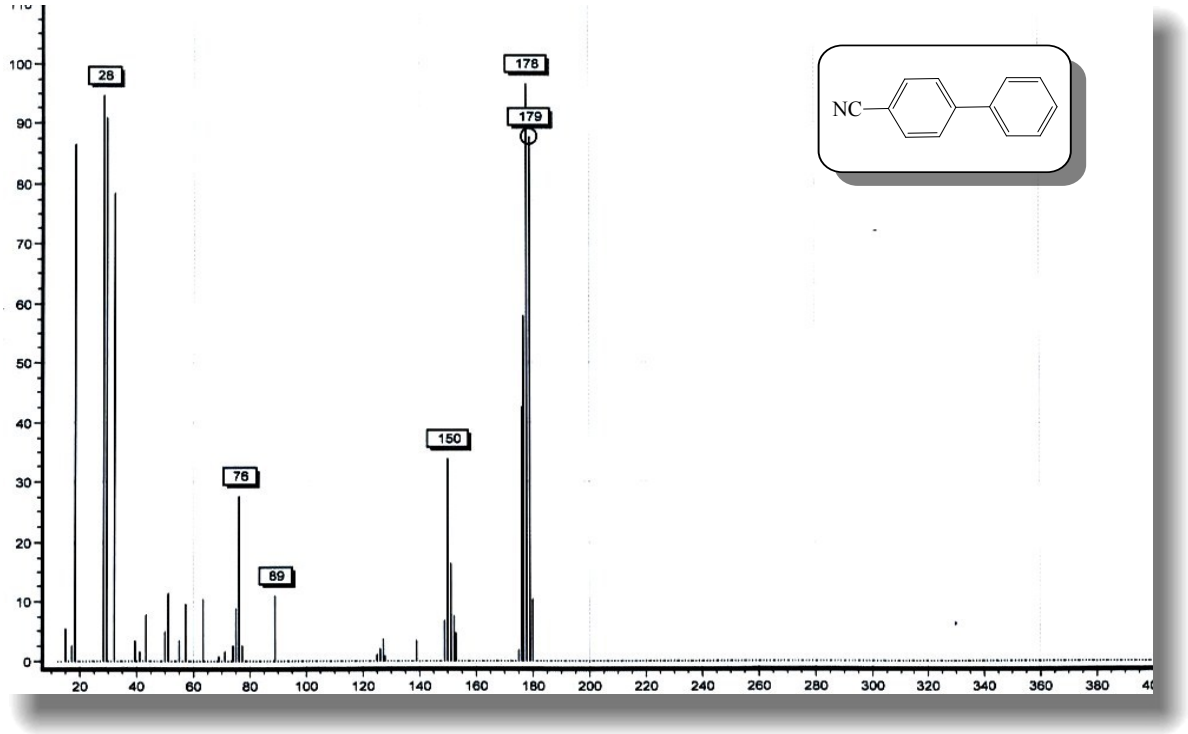

Figure 8-C: Mass spectrum of 4-Cyano-1, 1'-biphenyl (1j).

4-Phenylbenzaldehyde (1k): [9] Mp 62-63 ˚C (Lit. 62-63 ˚C); ^{1}H NMR (400 MHz, $CDCl_3$) δ 9.96 (s, 1H), 7.86 (d, *J* = 8.0 Hz, 2H), 7.66 (d, *J* = 8.0 Hz, 2H), 7.55 (d, *J*= 8.4 Hz, 2H), 7.39 (t, *J* = 7.2 Hz, 2H), 7.34 (t, *J* = 7.2 Hz, 1H); MS, *m/z* (%): 182 [M^+].

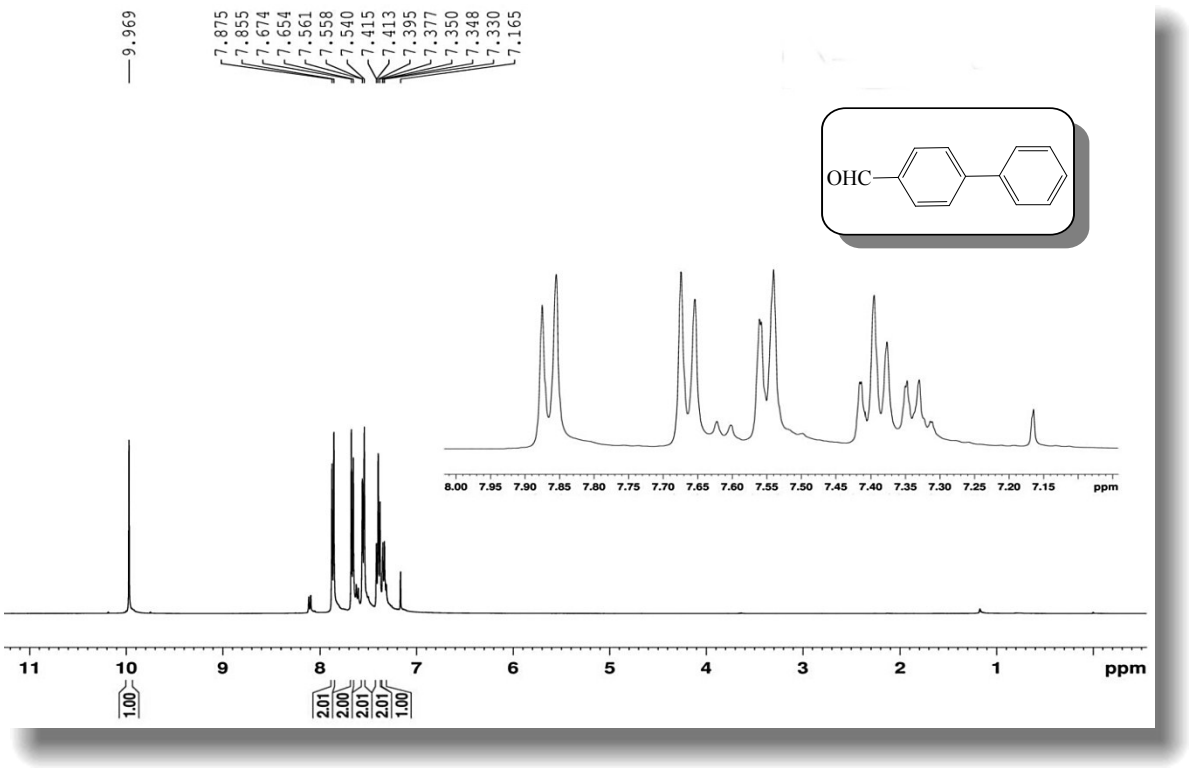

Figure 9-A: ^{1}H NMR (400 MHz, $CDCl_3$) of [1, 1'-biphenyl]-4-carbaldehyde (1k).

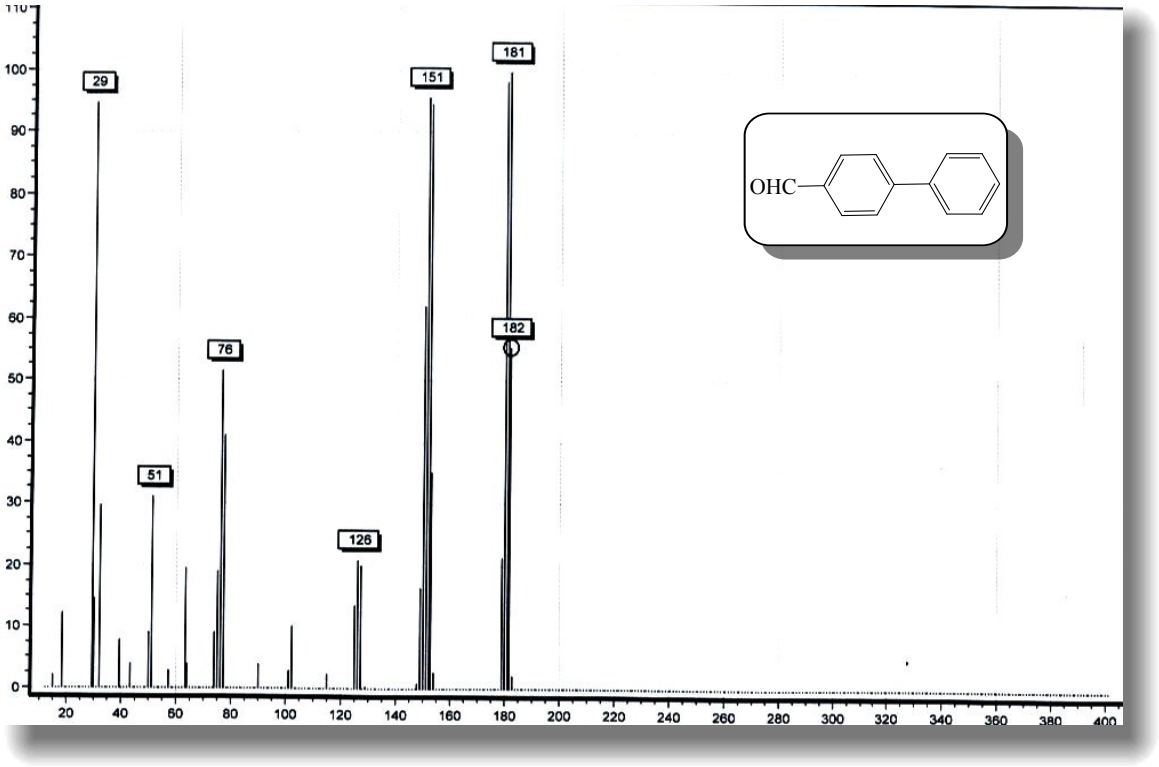

Figure 9-C: Mass spectrum of [1, 1'-biphenyl]-4-carbaldehyde (1k).

Biphenyl-3-carboxaldehyde (1l): [10] Mp 53-54 ˚C (Lit. 53-54 ˚C); ^{1}H NMR (500 MHz, $CDCl_3$) δ 10.11 (s, 1H), 8.13 (d, *J* = 1.5 Hz, 1H), 7.89 (dd, *J* = 7.5, 1.5 Hz, 2H), 7.66 -7.62 (m, 3H), 7.52 -7.49 (m, 2H), 7.43 (t, *J* = 7.5 Hz, 1H); MS, *m/z* (%): 182 [M^+].

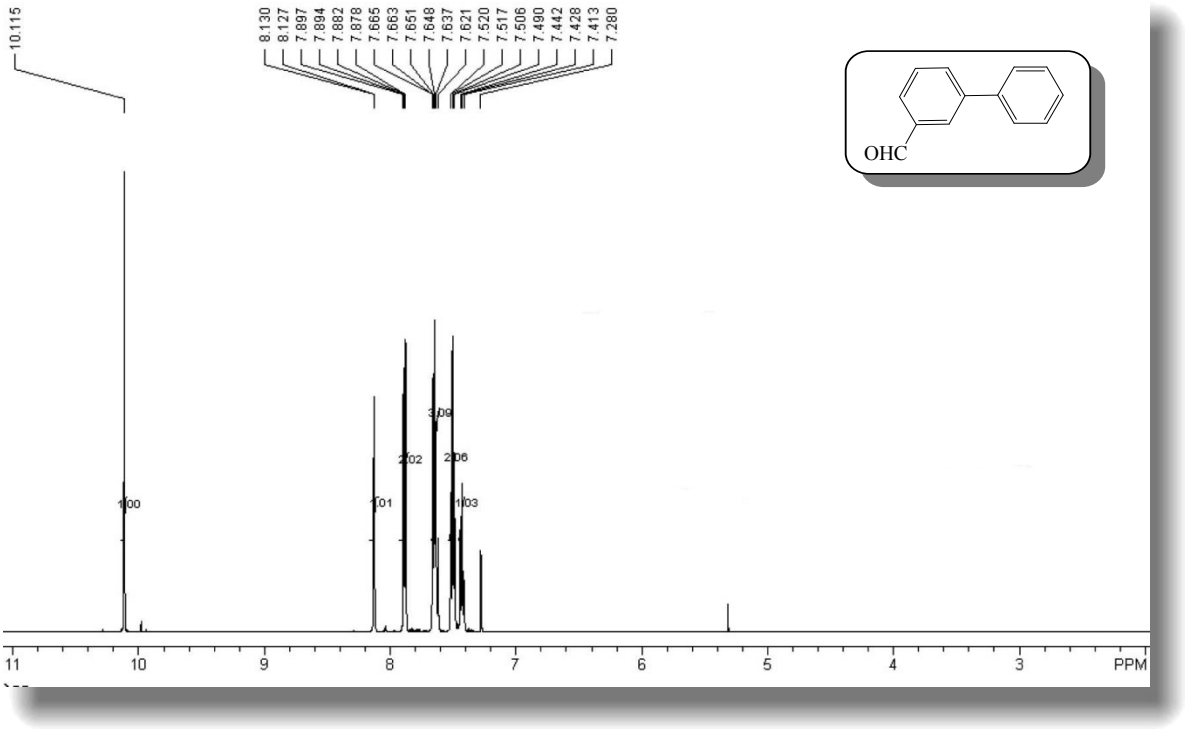

Figure 10-A: ^{1}H NMR (500 MHz, $CDCl_3$) of [1, 1'-biphenyl]-3-carbaldehyde (1l).

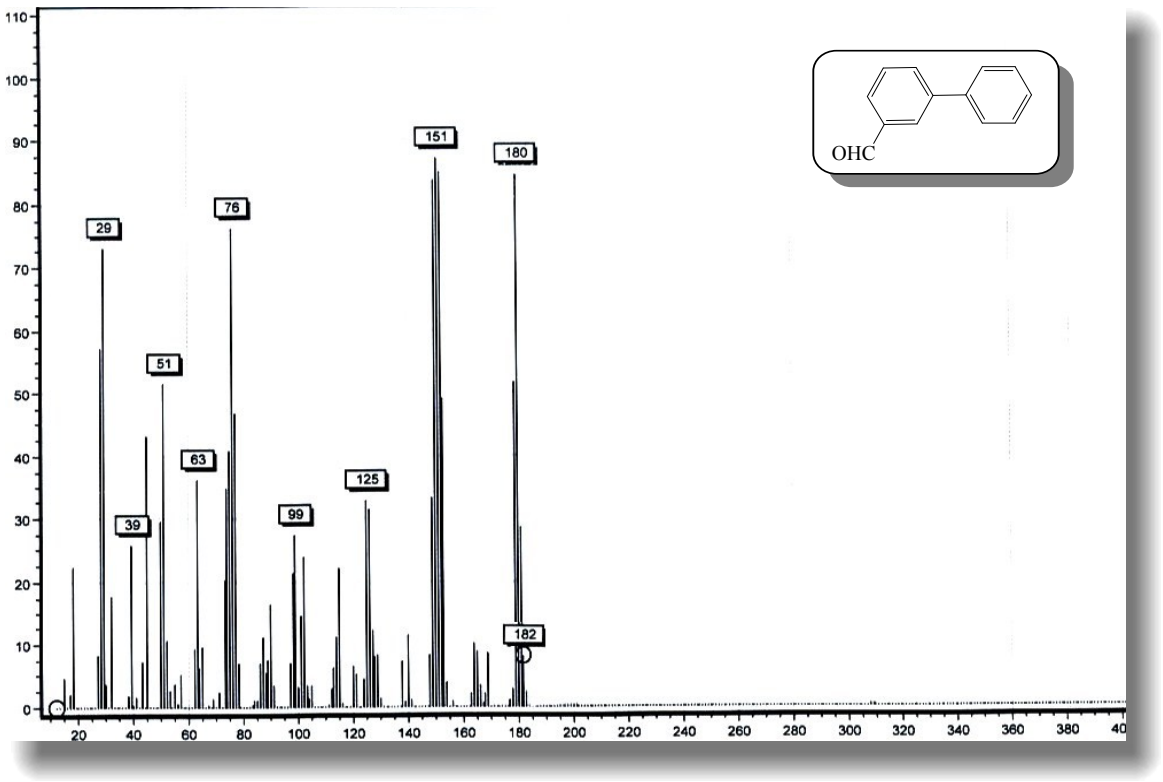

Figure 10-C: Mass spectrum of [1, 1'-biphenyl]-3-carbaldehyde (1l).

(*E*)-Methyl cinnamate (2a): [11] Mp 35-37 ˚C (Lit. 36-38 ˚C); ^{1}H NMR ($CDCl_3$, 400 MHz) δ 7.60 (d, *J* = 16.0 Hz, 1H), 7.44-7.41 (m, 2H), 7.29-7.27 (m, 3H), 6.35 (d, *J* = 16.0 Hz, 1H), 3.71 (s, 3H); ^{13}C NMR ($CDCl_3$, 100 MHz) δ 166.9, 144.4, 133.96, 129.8, 128.4, 127.6, 117.4, 51.2; MS, *m/z* (%): 162 [M^+].

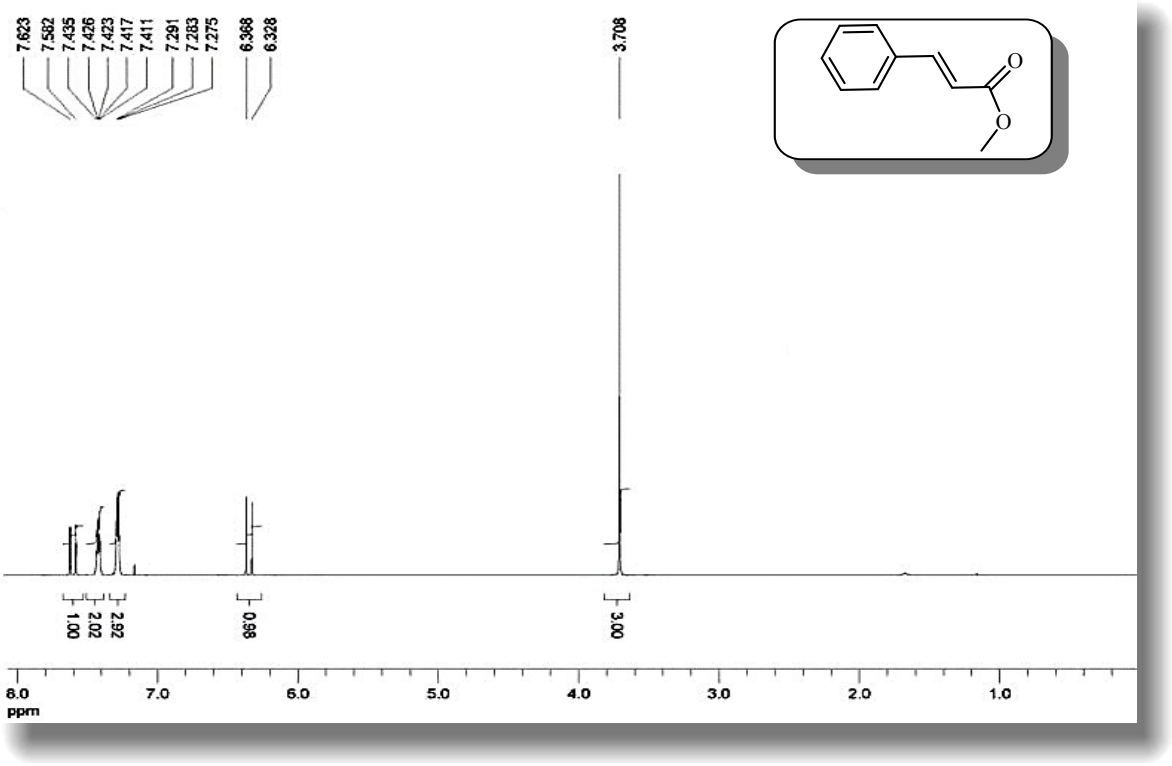

Figure 11-A: ^{1}H NMR (400 MHz, $CDCl_3$) of (*E*)-Methyl cinnamate (2a).

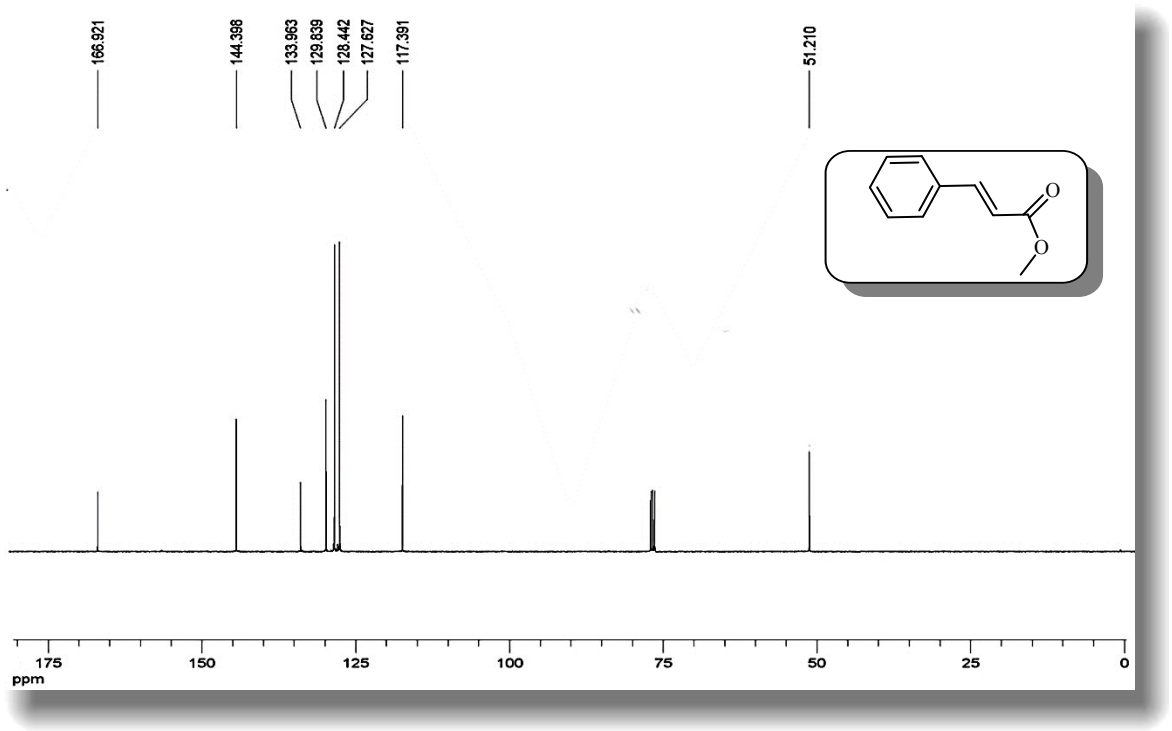

Figure 11-B: ^{13}C NMR (100 MHz, $CDCl_3$) of (*E*)-Methyl cinnamate (2a).

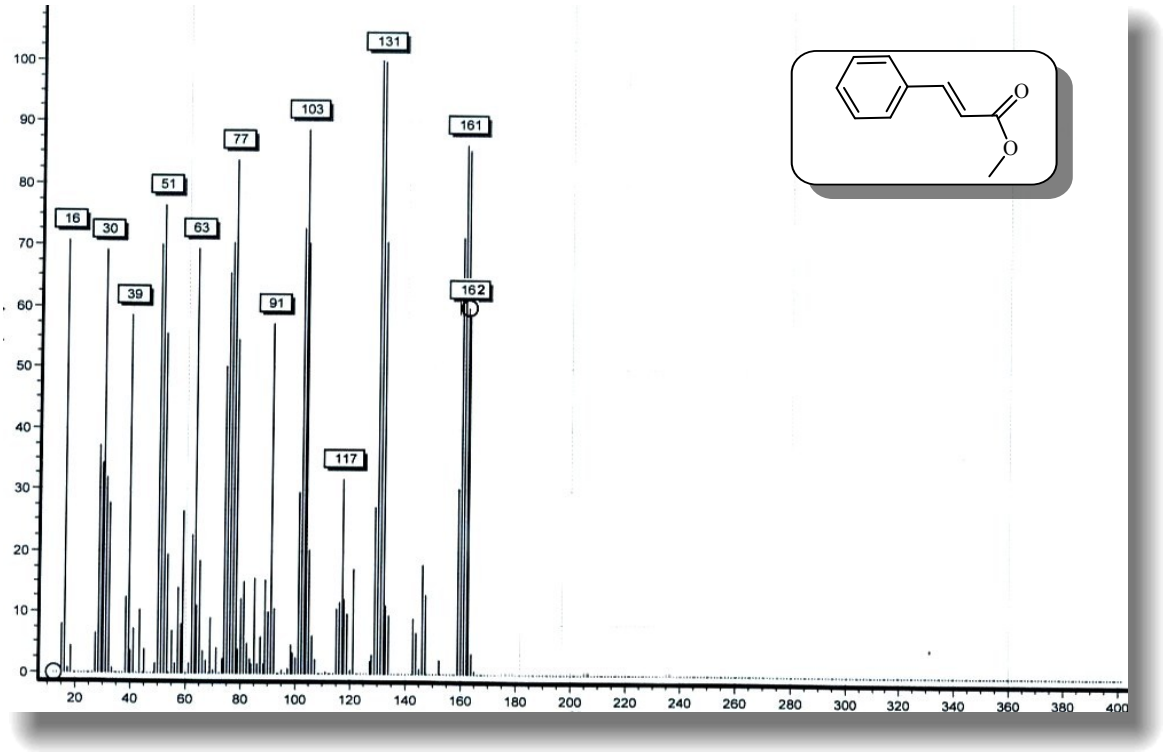

Figure 11-C: Mass spectrum of (*E*)-Methyl cinnamate (2a).

(*E*)-Methyl 3-(4-nitrophenyl) acrylate (2b): [11] Mp 160-162 °C (Lit. 160-162 °C); ^{1}H NMR ($CDCl_3$, 300 MHz): δ 8.25 (d, 2H, *J* = 8.8 Hz), 7.71 (s, 1H, *J* = 16.1 Hz), 7.68 (d, 2H, *J* = 8.7 Hz), 6.57 (d, 1H, *J* = 16.1 Hz), 3.84 (s, 3H); ^{13}C NMR ($CDCl_3$, 75 MHz): δ 52.3, 122.3, 124.4, 128.8, 140.7, 142.1, 148.7, 166.6; MS, *m/z* (%): 207 [M^+].

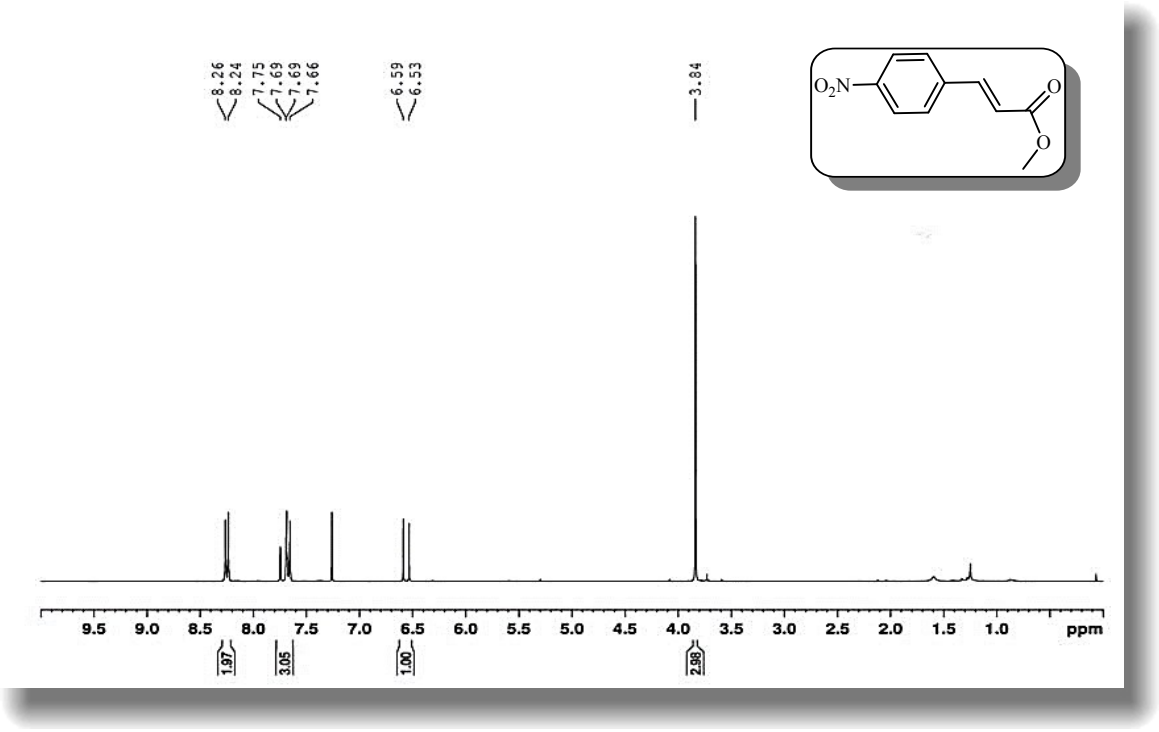

Figure 12-A: ^{1}H NMR (300 MHz, $CDCl_3$) of (*E*)-Methyl 3-(4-nitrophenyl) acrylate (2b).

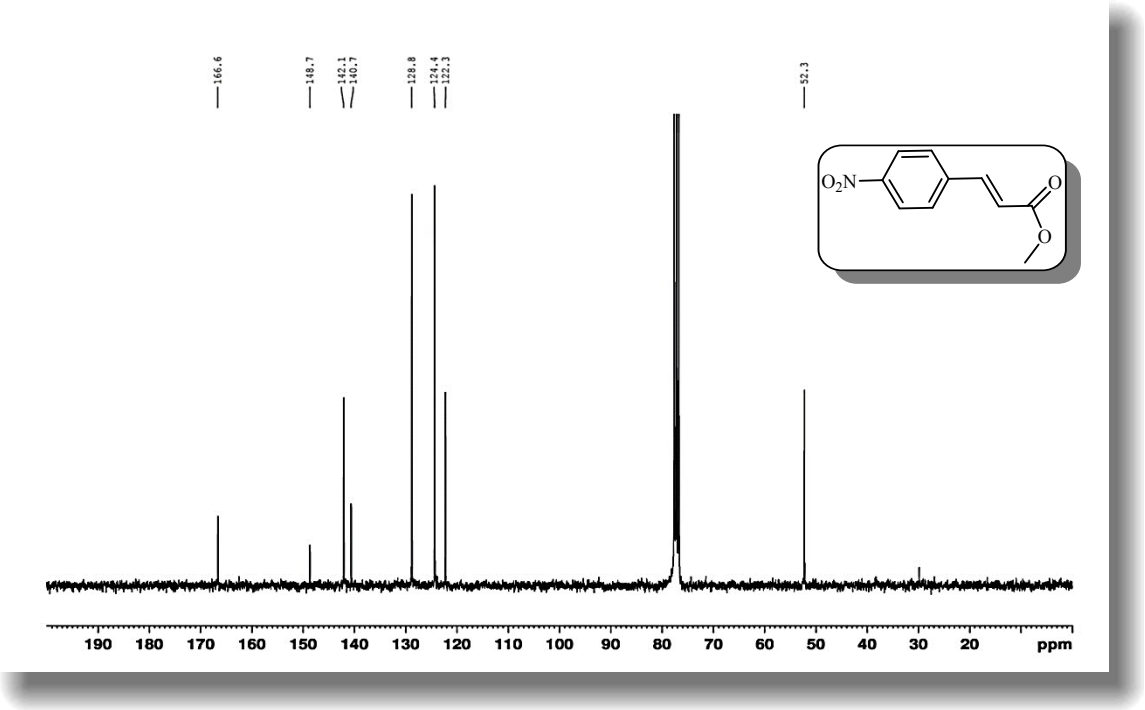

F

igure 12-B: ^{13}C NMR (75 MHz, $CDCl_3$) of (*E*)-Methyl 3-(4-nitrophenyl) acrylate (2b).

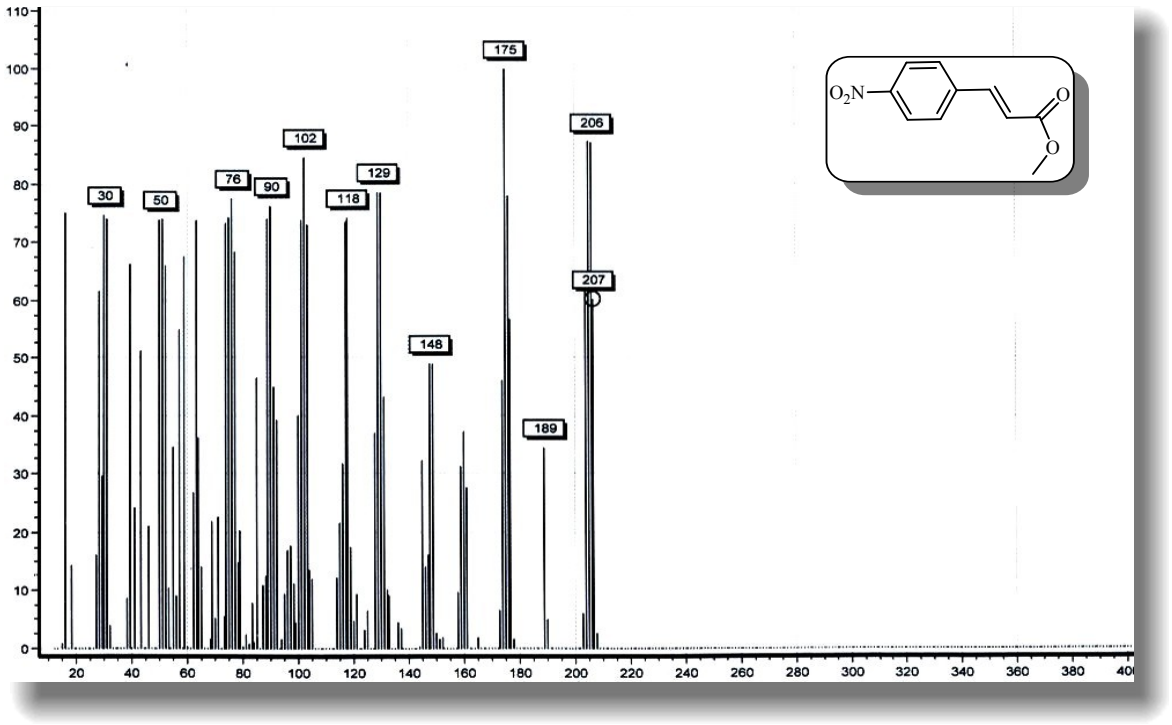

Figure 12-C: Mass spectrum of (*E*)-Methyl 3-(4-nitrophenyl) acrylate (2b).

(*E*)-Methyl 3-(4-chlorophenyl)acrylate (2c): [12] Mp 73-74 ˚C (Lit. 73-75˚C); ^{1}H NMR (300 MHz, $CDCl_3$): δ 7.63 (d, *J* = 16.0, 1H), 7.44 (d, *J* = 8.5, 2H), 7.35 (d, *J* = 8.6, 2H), 6.40 (d, *J* = 16.0, 1H), 3.80 (s, 3H); ^{13}C NMR (75 MHz, $CDCl_3$) δ 167.2, 143.4, 136.3, 133.0, 129.3, 129.3, 118.5, 51.8; MS, *m/z* (%): 196 [M^+].

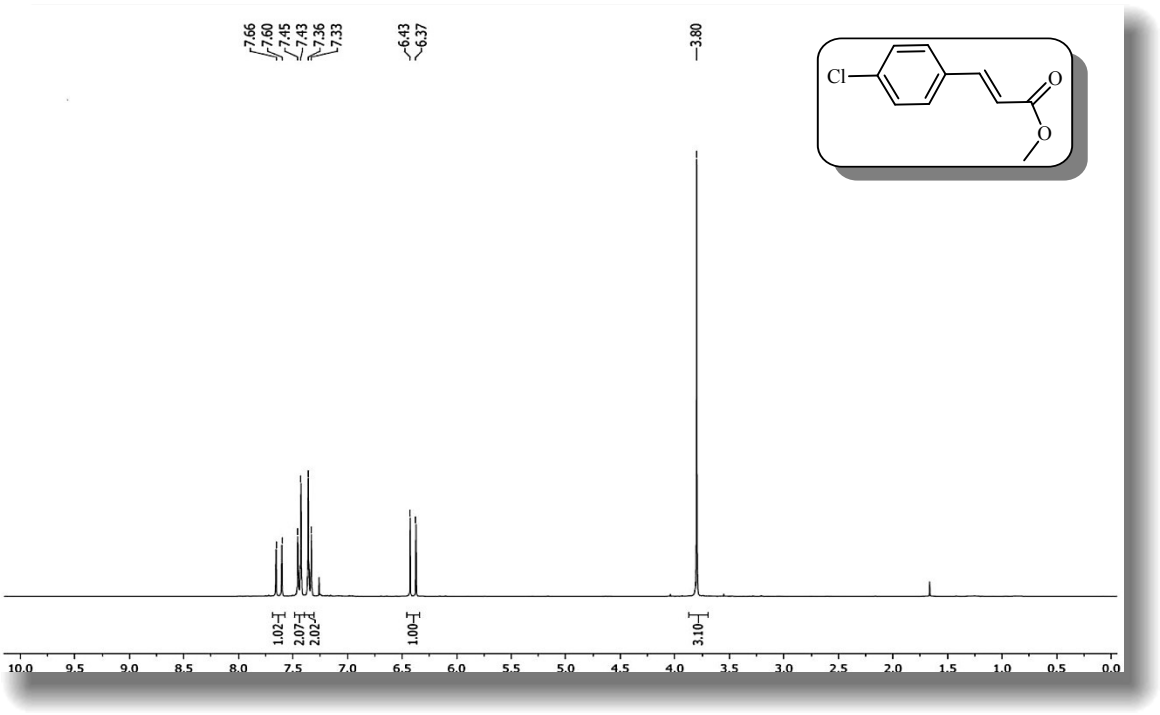

Figure 13-A: ^{1}H NMR (300 MHz, $CDCl_3$) of (*E*)-Methyl 3-(4-chlorophenyl)acrylate (2c).

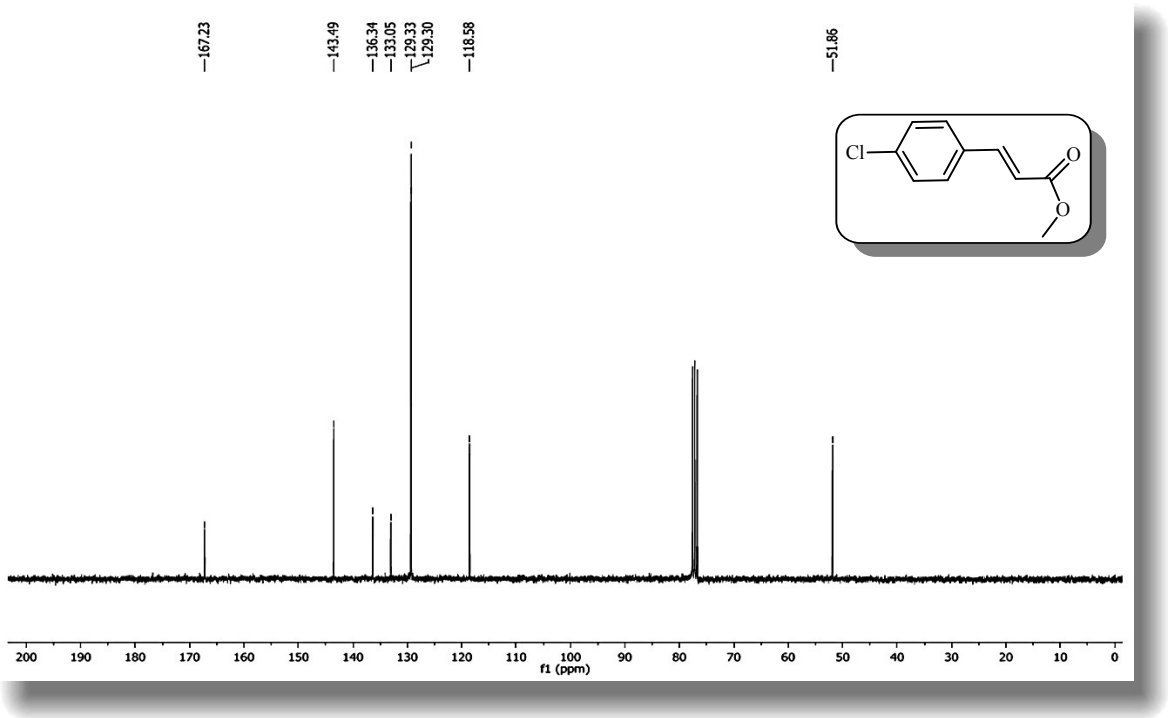

Figure 13-B: ^{13}C NMR (75 MHz, $CDCl_3$) of (*E*)-Methyl 3-(4-chlorophenyl)acrylate (2c).

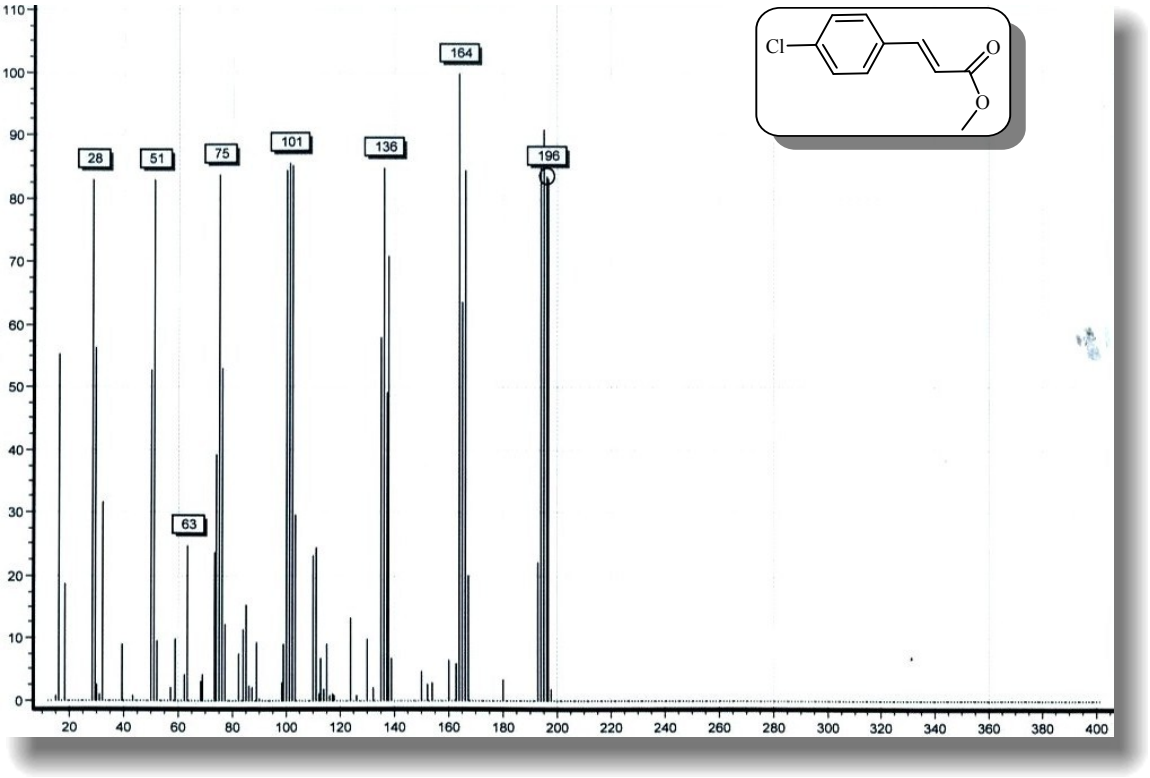

F

igure 13-C: Mass spectrum of (*E*)-Methyl 3-(4-chlorophenyl)acrylate (2c).

(*E*)-Methyl 3-(4-methoxyphenyl)acrylate (2d): [13] Mp 88-91 ˚C (Lit. 88-89 ˚C); ^{1}H NMR ($CDCl_3$, 400 MHz): δ 7.67 (d, *J* = 16.0 Hz, 1H), 7.50-7.47 (m, 2H), 6.94-6.90 (m, 2H), 6.33 (d, *J* = 16.0 Hz, 1H), 3.86 (s, 3H), 3.81 (s, 3H); ^{13}C NMR ($CDCl_3$, 100 MHz): δ 167.8, 161.5, 144.6, 129.8, 127.2, 115.5, 114.4, 55.5, 51.6; MS, *m/z* (%): 192 [M^+].

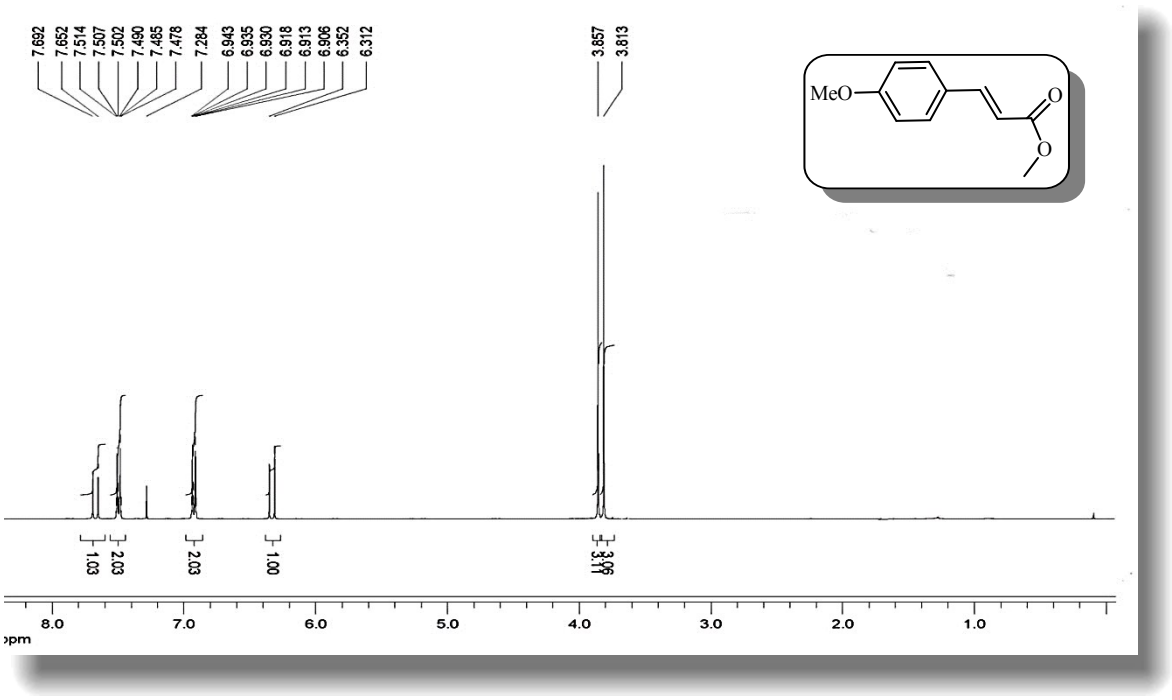

Figure 14-A: ^{1}H NMR (400 MHz, $CDCl_3$) of (*E*)-Methyl 3-(4-methoxyphenyl)acrylate (2d).

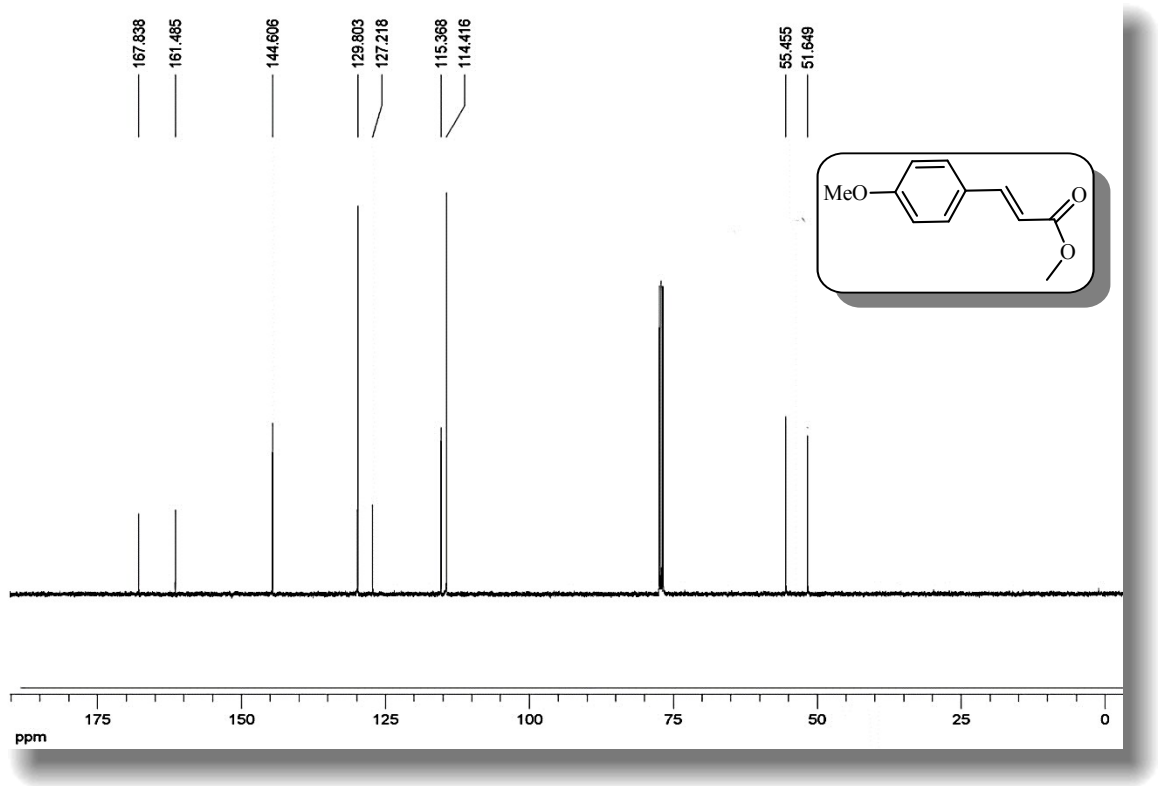

F

igure 14-B: ^{13}C NMR (100 MHz, $CDCl_3$) of (*E*)-Methyl 3-(4-methoxyphenyl)acrylate (2d).

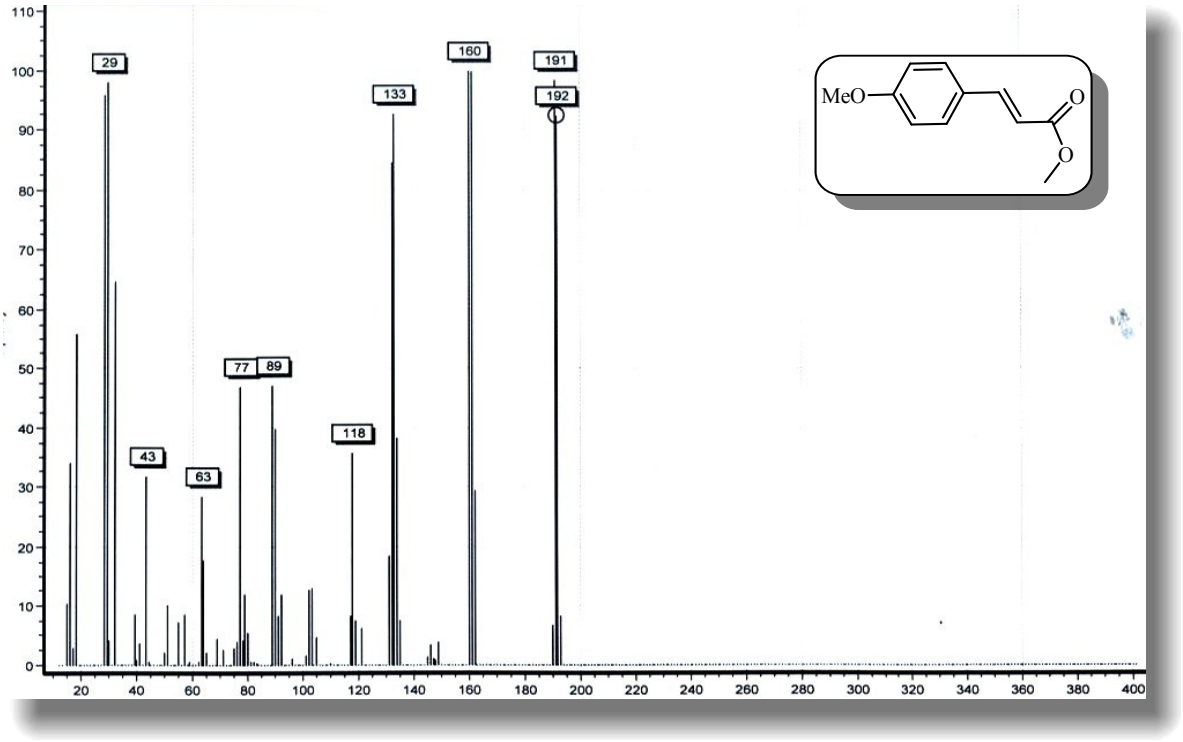

Figure 14-C: Mass spectrum of (*E*)-Methyl 3-(4-methoxyphenyl)acrylate (2d).

(*E*)-Methyl 3-(*p*-tolyl) acrylate (2e): [14] Mp 55-57 ˚C (Lit. 56-57 ˚C); ^{1}H NMR ($CDCl_3$, 400 MHz); δ 7.69 (d, *J* = 16.0 Hz, 1H), 7.44-7.42 (m, 2H), 7.21-7.19 (m, 2H), 6.42 (d, *J* = 16.0 Hz, 1H), 3.81(s, 3H), 2.39 (s, 3H); ^{13}C NMR ($CDCl_3$, 100 MHz): δ 167.6, 144.9., 140.7, 131.7, 129.6, 128.0, 116.7, 51.6, 21.5; MS, *m/z* (%): 177 [M^+].

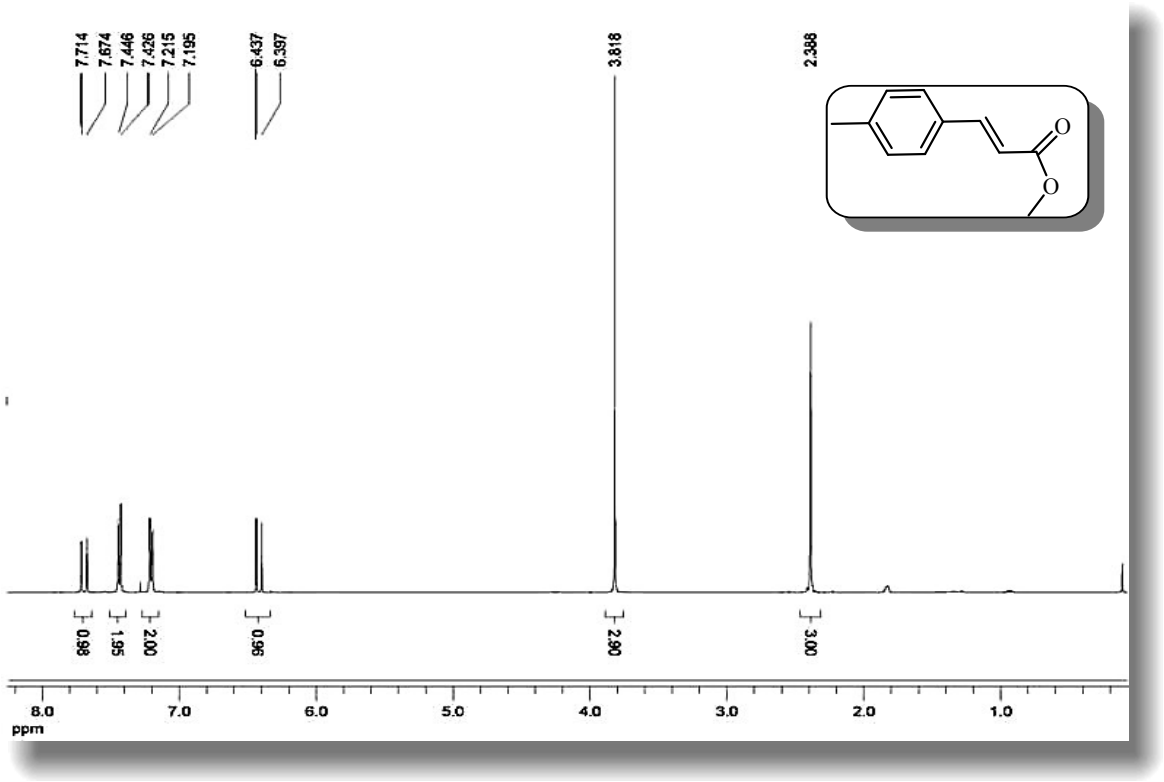

Figure 15-A: ^{1}H NMR (400 MHz, $CDCl_3$) of (*E*)-Methyl 3-(*p*-tolyl) acrylate (2e).

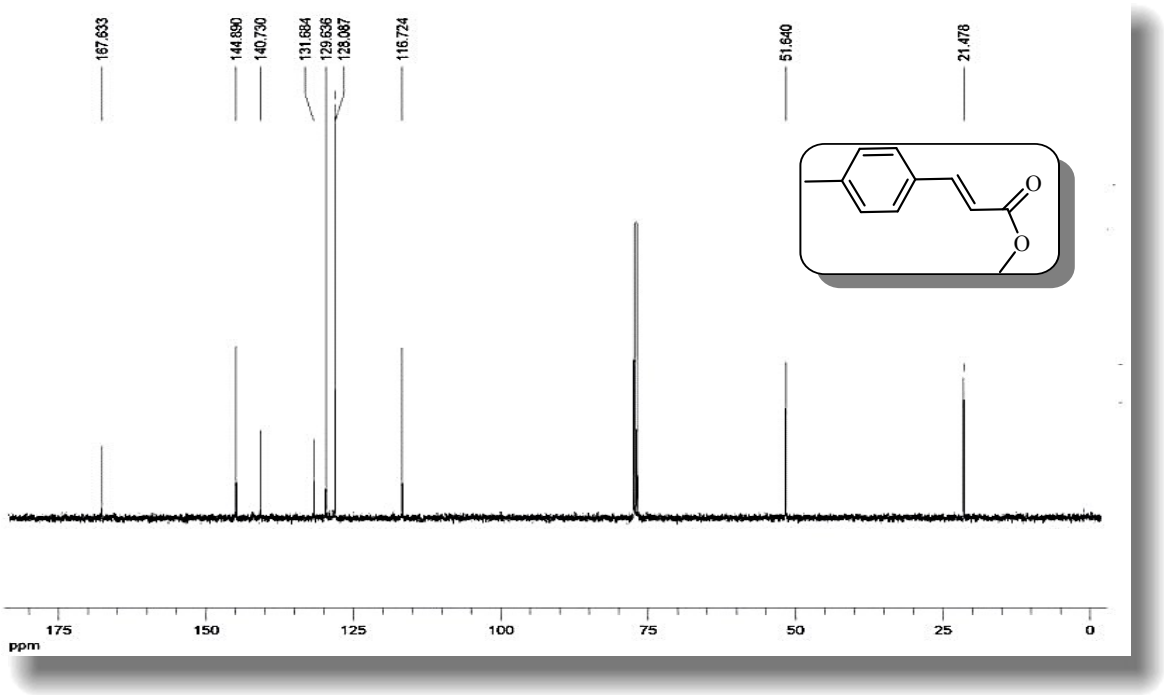

Figure 15-B: ^{13}C NMR (100 MHz, $CDCl_3$) of (*E*)-Methyl 3-(*p*-tolyl) acrylate (2e).

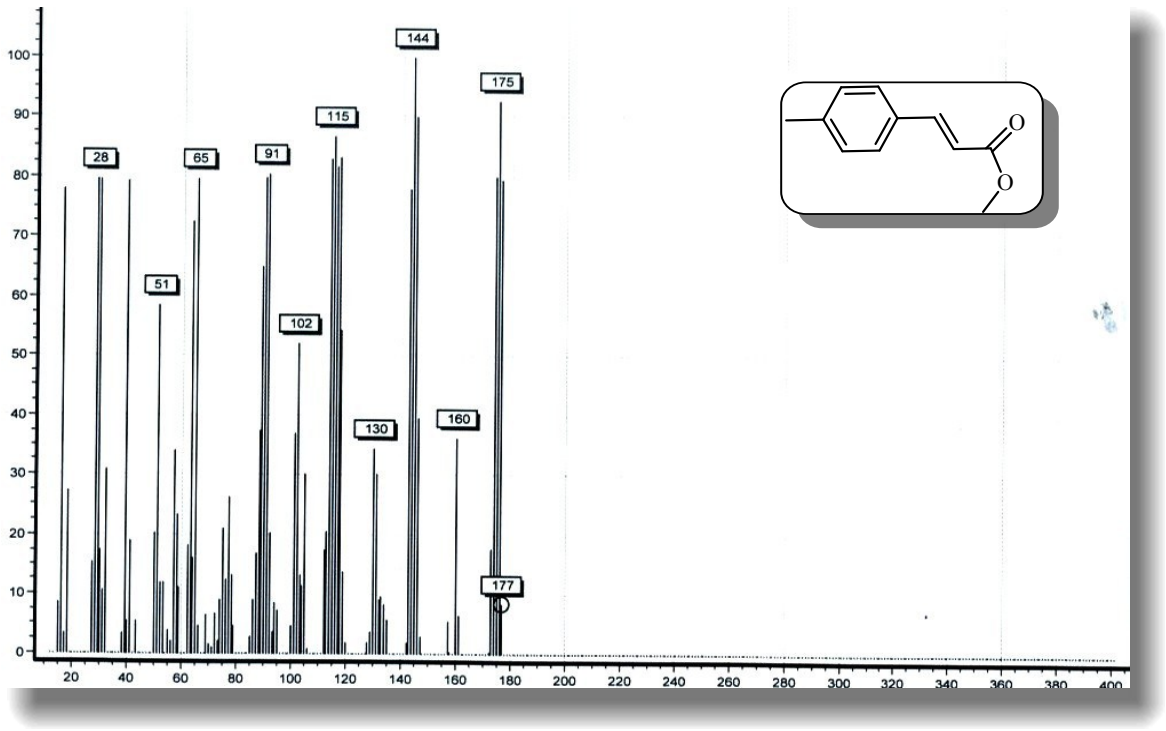

Figure 15-C: Mass spectrum of (*E*)-Methyl 3-(*p*-tolyl) acrylate (2e).

(*E*)-Methyl 3-(4-cyanophenyl)acrylate (2i): [13] Mp 122-125 ˚C (Lit. 122-126 ˚C); ^{1}H NMR (300 MHz, $CDCl_3$): δ 7.67 (d, *J* = 8.4, 2H), 7.66 (d, *J* = 16.1, 1H), 7.60 (d, *J* = 8.3, 2H), 6.51 (d, *J* = 16.0, 1H), 3.82 (s, 3H); ^{13}C NMR (75 MHz, $CDCl_3$): δ 166.6, 142.5, 138.8, 132.7, 128.5, 121.5, 118.4, 113.6, 52.0; MS, *m/z* (%): 187 [M^+].

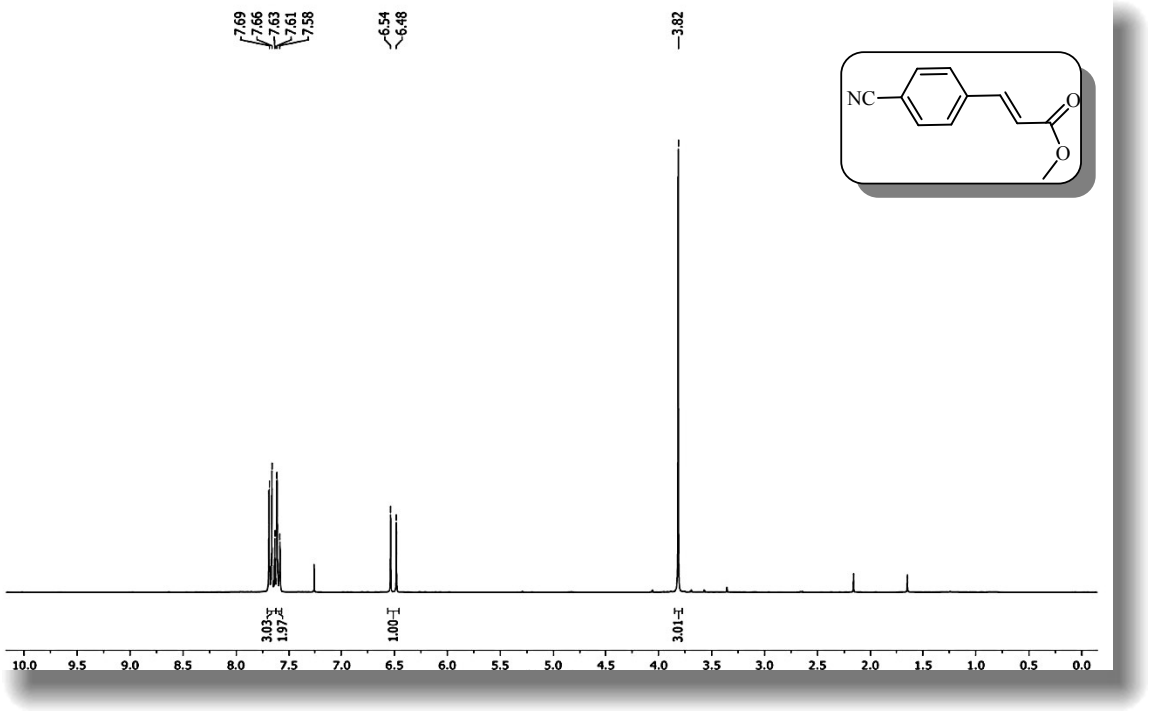

F

igure 16-A: ^{1}H NMR (300 MHz, $CDCl_3$) of (*E*)-Methyl 3-(4-cyanophenyl)acrylate (2i).

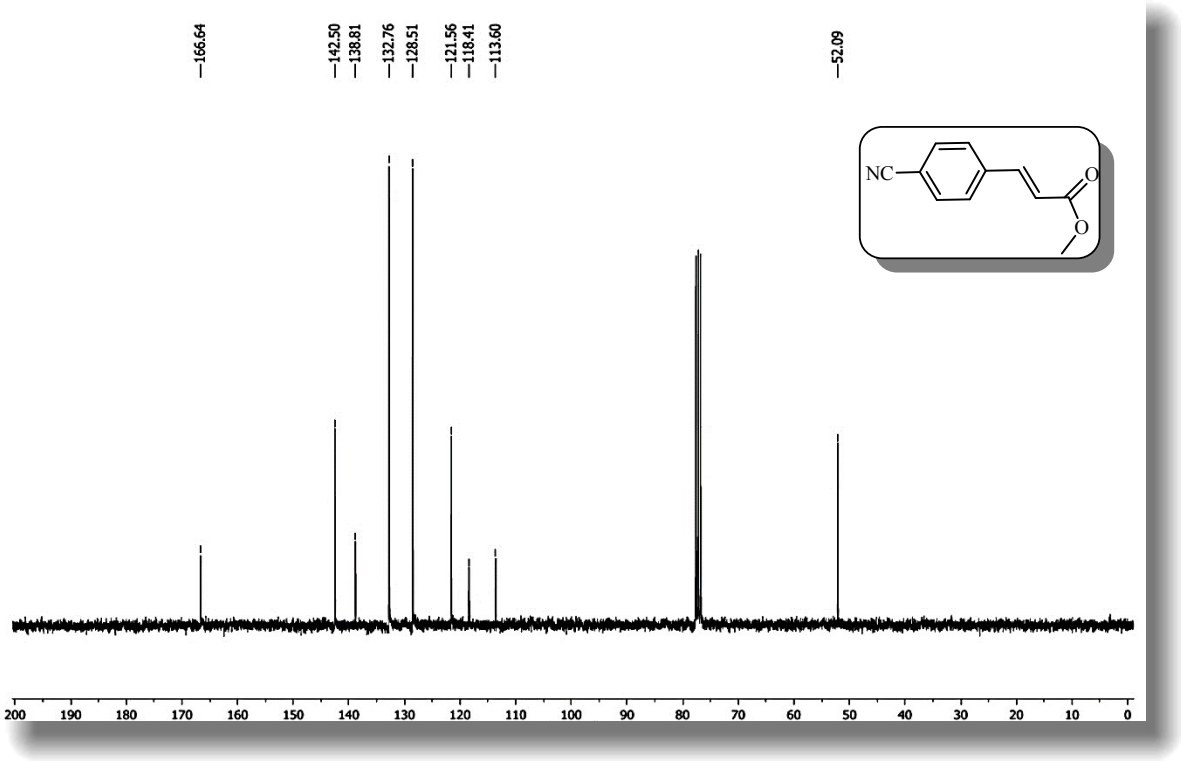

Figure 16-B: ^{13}C NMR (75 MHz, $CDCl_3$) of (*E*)-Methyl 3-(4-cyanophenyl)acrylate (2i).

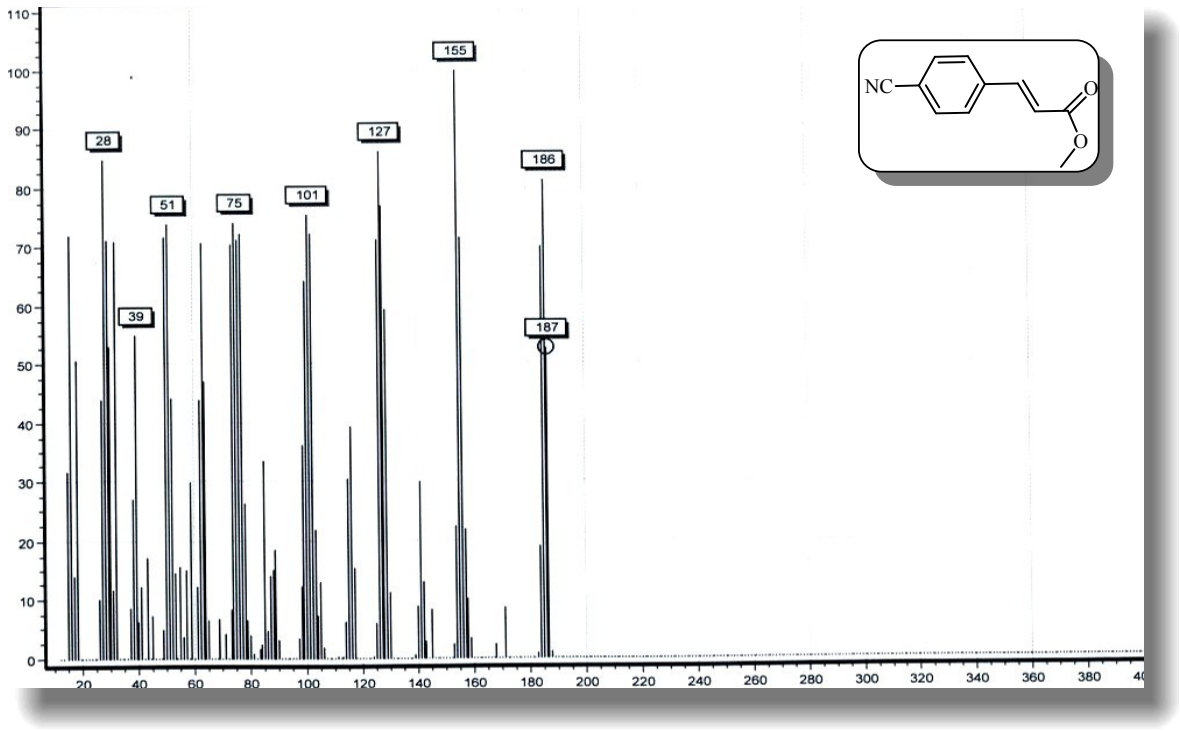

Figure 16-C: Mass spectrum of (*E*)-Methyl 3-(4-cyanophenyl)acrylate (2i).

(*E*)-Butyl cinnamate (2j): [15] Oil; ^{1}H NMR (400 MHz, $CDCl_3$) δ 7.60 (1H, d, *J* = 16.4 Hz, CHPh), 7.43 -7.45 (2H, m, Ph), 7.28 -7.31 (3H, m, Ph), 6.36 (1H, d, *J* = 16.0 Hz, CHCO), 4.13 (2H, t, *J* = 6.8 Hz, OCH_2), 1.59 -1.62 (2H, m, $MeCH_2CH_2$), 1.34 -1.36 (2H, m, $MeCH_2$), 0.88 (3H, t, *J* = 7.6 Hz, Me); ^{13}C NMR (100 MHz, $CDCl_3$) δ 13.7, 19.2, 30.8, 64.3, 118.2, 128.0, 128.8, 130.1, 134.4, 144.4, 166.8.

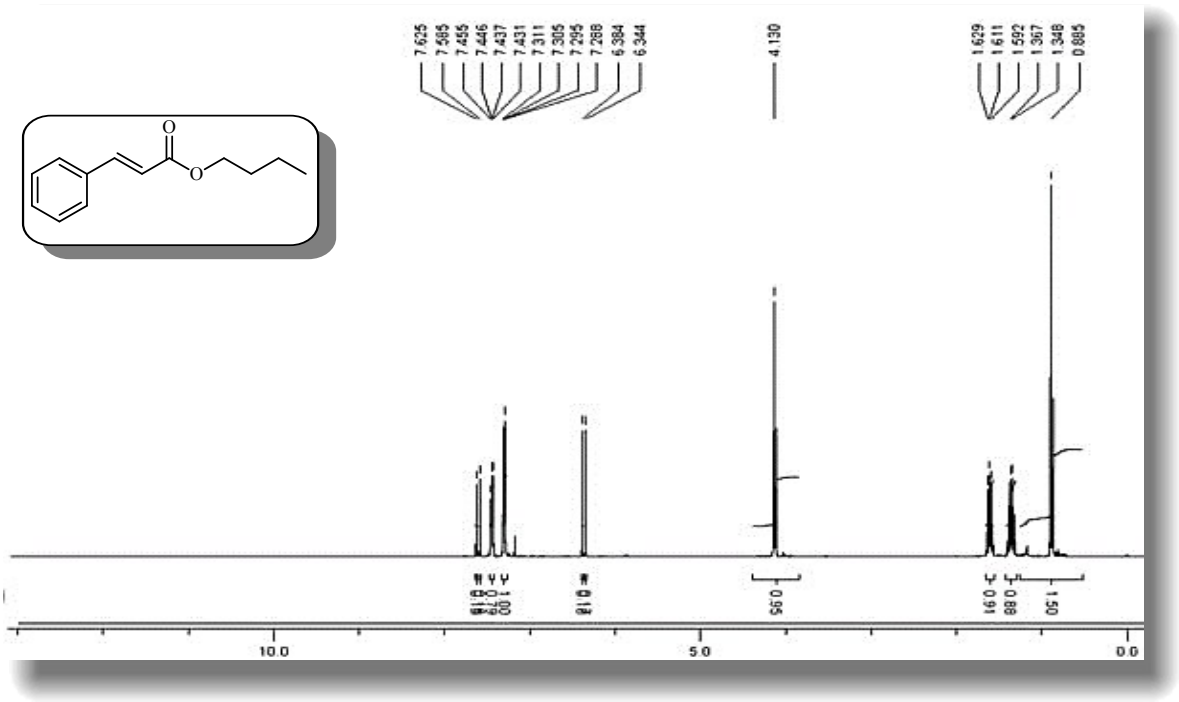

Figure 17-A: ^{1}H NMR (400 MHz, $CDCl_3$) of (*E*)-Butyl cinnamate (2j).

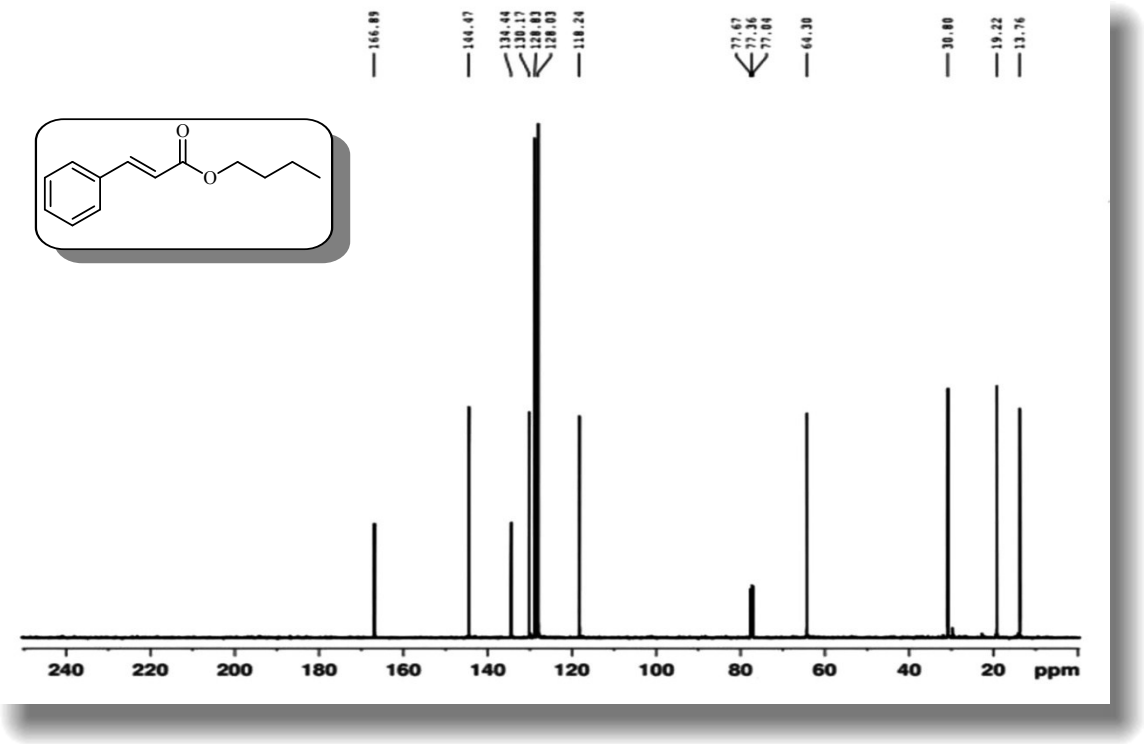

F

igure 17-B: ^{13}C NMR (100 MHz, $CDCl_3$) of (*E*)-Butyl cinnamate (2j).

(*E*)-Butyl 3-(4-nitrophenyl)acrylate (2k): [16] Mp 67-69 ˚C (Lit. 59-64˚C); ^{1}H NMR (400 MHz, $CDCl_3$) δ 8.20 (2H, d, *J* = 8.0 Hz, Ph), 7.63-7.68 (3H, m, Ph and CHAr), 6.53 (1H, d, *J* = 16.0 Hz, CHCO), 4.17-4.24 (2H, m, OCH_2), 1.62-1.69 (2H, m, $MeCH_2CH_2$), 1.35-1.44 (2H, m, $MeCH_2$), 0.92 (3H, t, *J* = 7.2 Hz, Me); ^{13}C NMR (100 MHz, $CDCl_3$) δ 13.6, 19.1, 30.6, 64.7, 122.5, 124.0, 128.6, 140.5, 141.5, 148.3, 166.0.

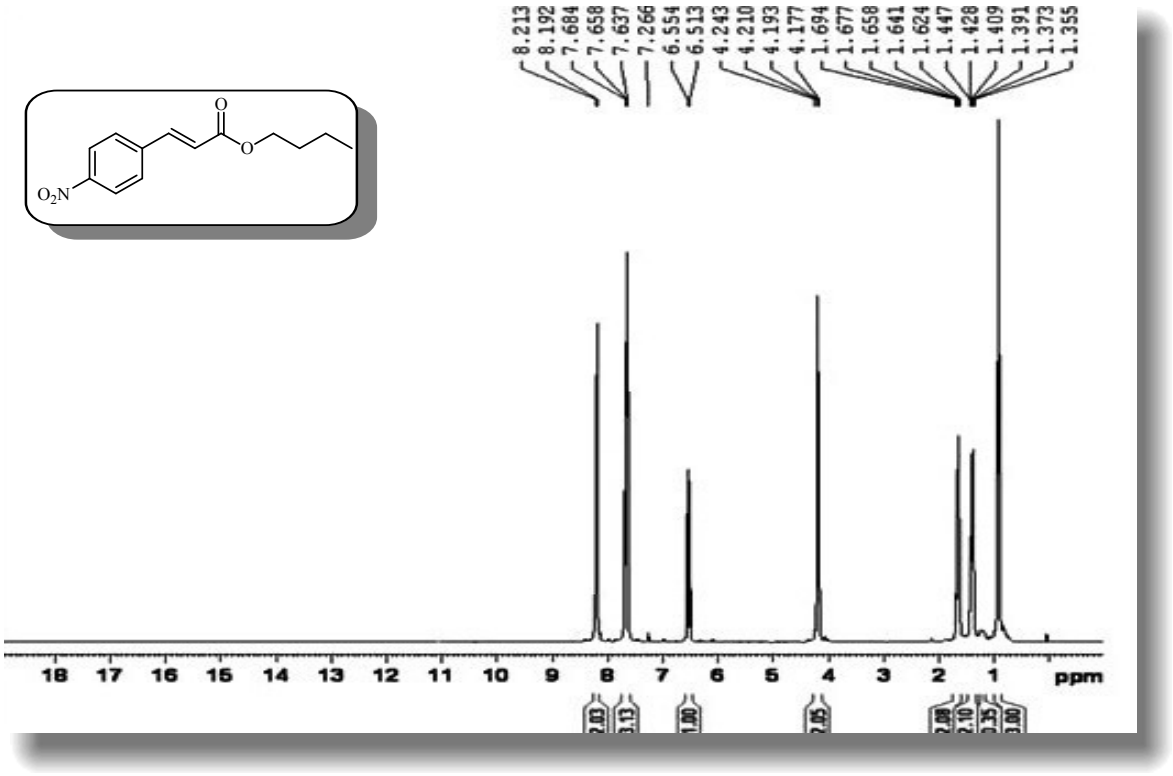

Figure 18-A: ^{1}H NMR (400 MHz, $CDCl_3$) of (*E*)-Butyl 3-(4-nitrophenyl) acrylate (2k).

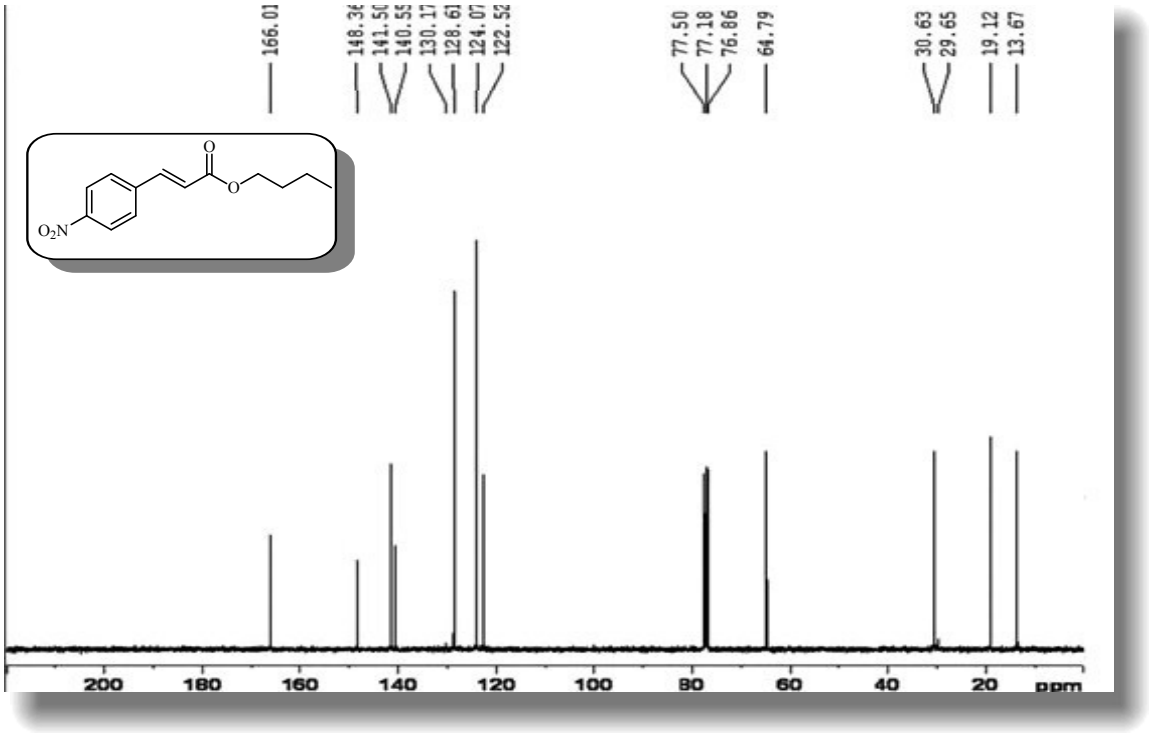

Figure 18-B: ^{13}C NMR (100 MHz, $CDCl_3$) of (*E*)-Butyl 3-(4-nitrophenyl) acrylate (2k).

(*E*)-*n*-Butyl-3-(4-chlorophenyl)acrylate (2l): [17] Mp 37-39 ˚C (Lit. 38-40 ˚C); ^{1}H NMR (400 MHz, $CDCl_3$) δ 7.62 (d, *J* = 16.0 Hz, 1H), 7.45 (d, *J* = 8.3 Hz, 2H), 7.35 (d, *J* = 8.4 Hz, 2H), 6.41 (d, *J* = 16.0 Hz, 1H), 4.21 (t, *J* = 6.7 Hz, 2H), 1.72-1.65 (m, 2H), 1.44 (dq, *J* = 14.7, 7.4 Hz, 2H), 0.96 (t, *J* = 7.4 Hz, 3H); ^{13}C NMR (100 MHz, $CDCl_3$) δ 166.8, 143.1, 136.1, 133.0, 129.2, 129.2, 118.9, 64.6, 30.7, 19.2, 13.7.

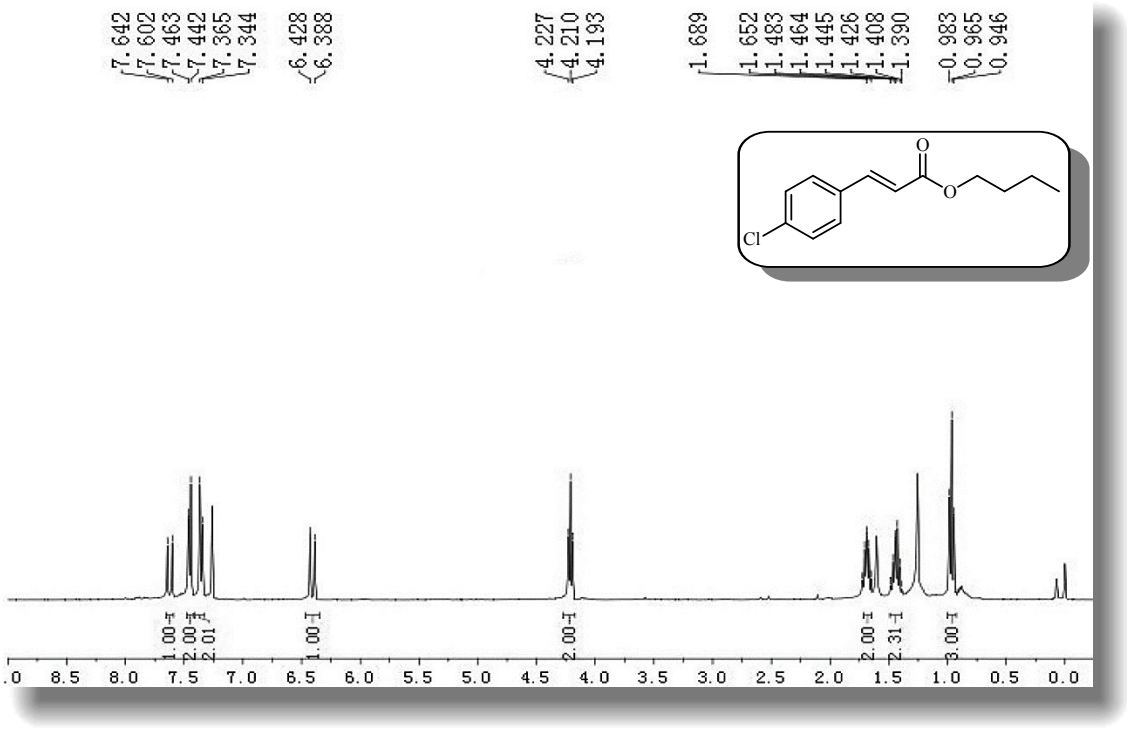

Figure 19-A: ^{1}H NMR (400 MHz, $CDCl_3$) of (*E*)-Butyl 3-(4-chlorophenyl) acrylate (2l).

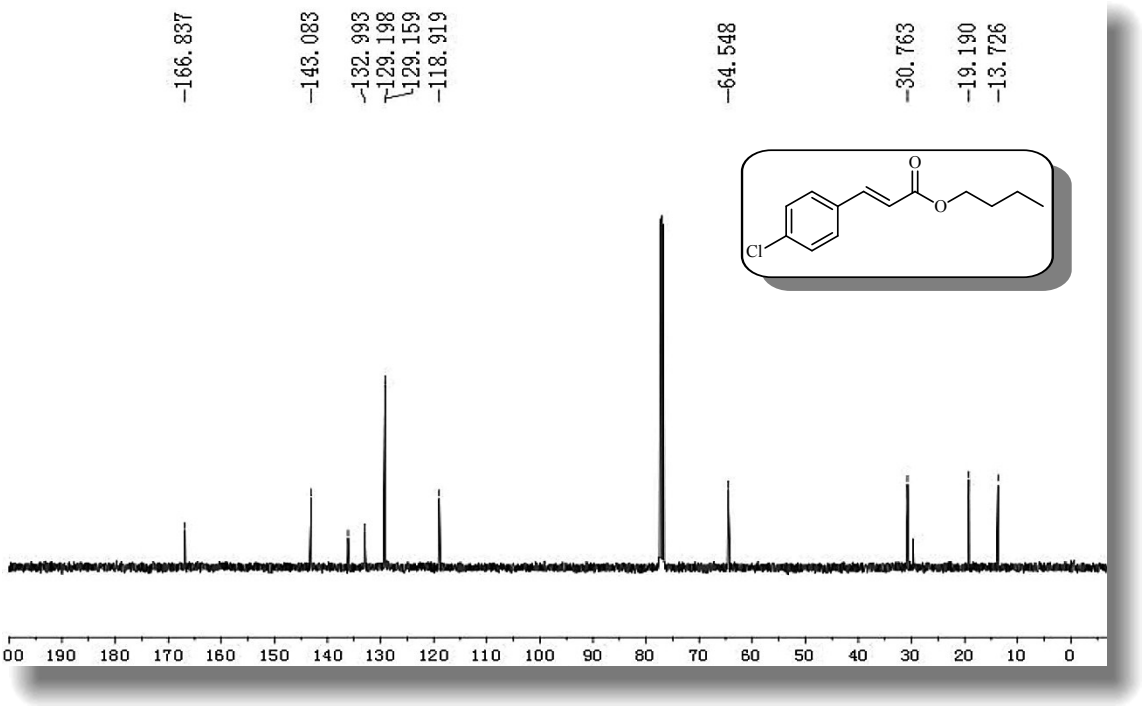

Figure 19-B: ^{13}C NMR (100 MHz, $CDCl_3$) of (*E*)-Butyl 3-(4-chlorophenyl) acrylate (2l).

(*E*)-Butyl 3-(4-methoxyphenyl)acrylate (2m): [18] Mp 90-92 ˚C (Lit. 92-93 ˚C); ^1H NMR (400 MHz, $CDCl_3$) δ 7.58 (1H, d, *J*= 16.0 Hz, CHAr), 7.39 (2H, d, *J*= 4.2 Hz, Ph), 6.81 (2H, d, *J*= 4.8 Hz, Ph), 6.24 (1H, d, *J*= 16.0 Hz, CHCO), 4.13 (2H, t, *J*= 7.0 Hz, OCH_2), 3.72 (3H, s, OMe), 1.60-1.62 (2H, m, $MeCH_2CH_2$), 1.35-1.40 (2H, m, $MeCH_2$), 0.91 (3H, t, *J*= 7.0 Hz, Me); ^{13}C NMR (100 MHz, $CDCl_3$) δ 51.64, 55.0,114.1,115.5,127.0,129.5, 144.0, 161.2, 167.1; MS (EI): *m/z* = 234 [M^+].

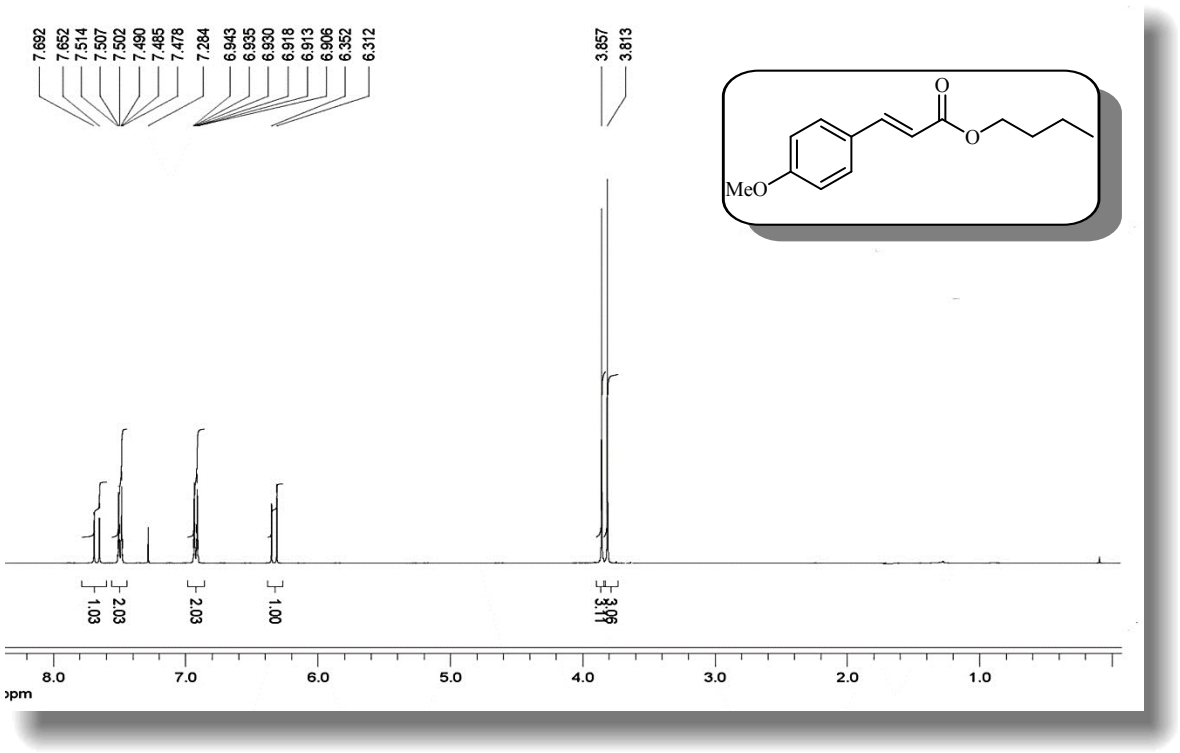

Figure 20-A: ^{1}H NMR (400 MHz, $CDCl_3$) of (*E*)-Butyl 3-(4-methoxyphenyl) acrylate (2m).

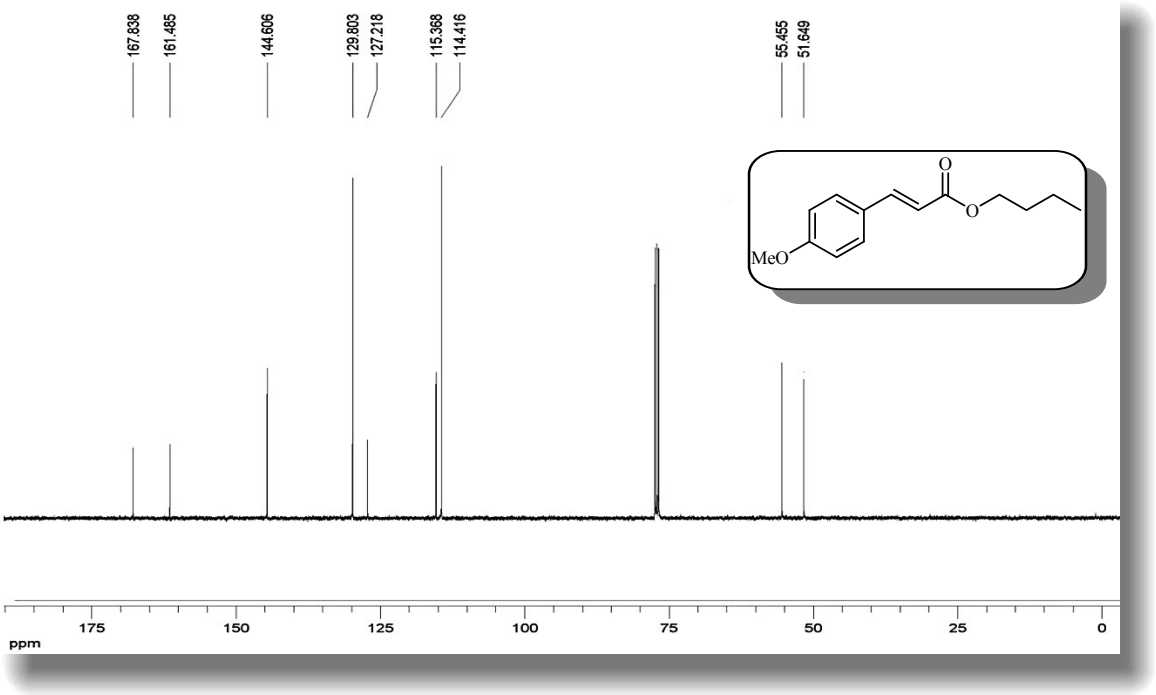

Figure 20-B: ^{13}C NMR (100 MHz, $CDCl_3$) of (*E*)-Butyl 3-(4-methoxyphenyl) acrylate (2m).

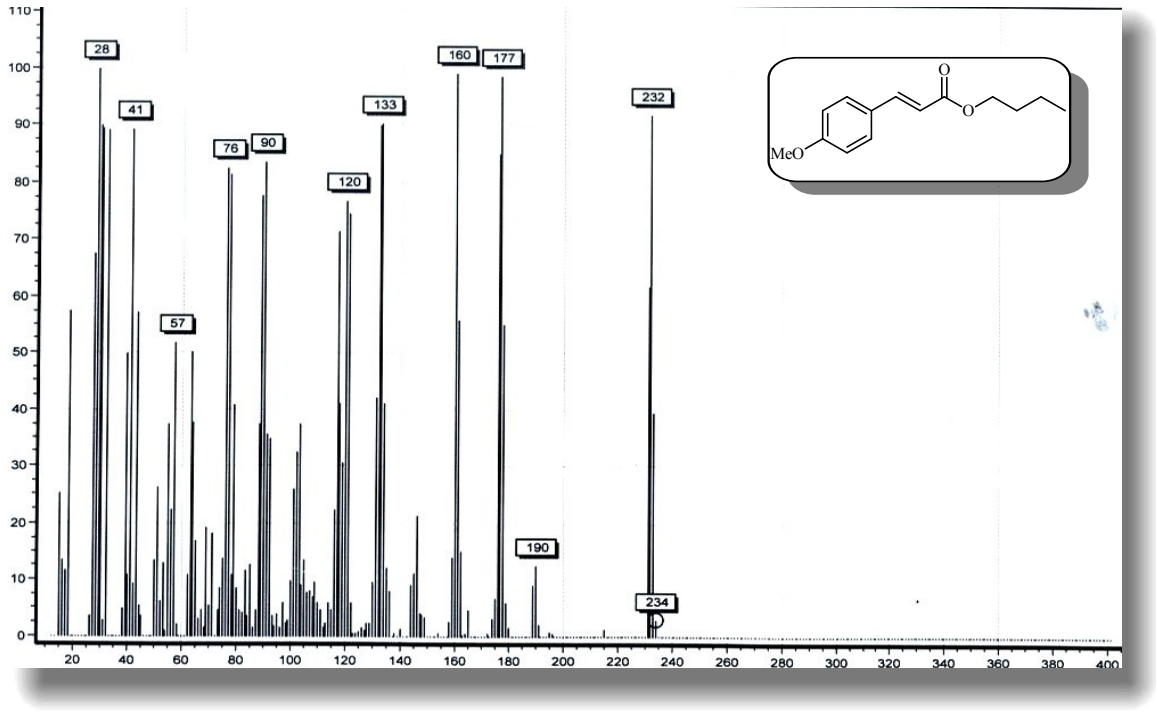

Figure 20-C: Mass spectrum of (*E*)-Butyl 3-(4-methoxyphenyl) acrylate (2m).

(*E*)-Butyl 3-(*p*-tolyl)acrylate (2n): [19] Oil; ^{1}H NMR (400 MHz, $CDCl_3$) δ 7.52 (1H, d, *J* = 18.2 Hz, CHAr), 7.28-7.32 (2H, m, Ph), 7.04-7.07 (2H, m, Ph), 6.30 (1H, d, *J* = 16 Hz, CHCO), 4.09 (2H, t, *J* = 5.0 Hz, OCH_2), 2.24 (3H, s, MePh), 1.32-1.40 (2H, m, $MeCH_2CH_2$), 1.23-1.31 (2H, m, $MeCH_2$), 0.85 (3H, t, *J* = 7.4 Hz, Me); ^{13}C NMR (100 MHz, $CDCl_3$) δ 13.7, 19.2, 21.4, 30.8, 64.2, 117.1, 128.0, 129.5, 131.7, 140.5, 144.5, 167.2.

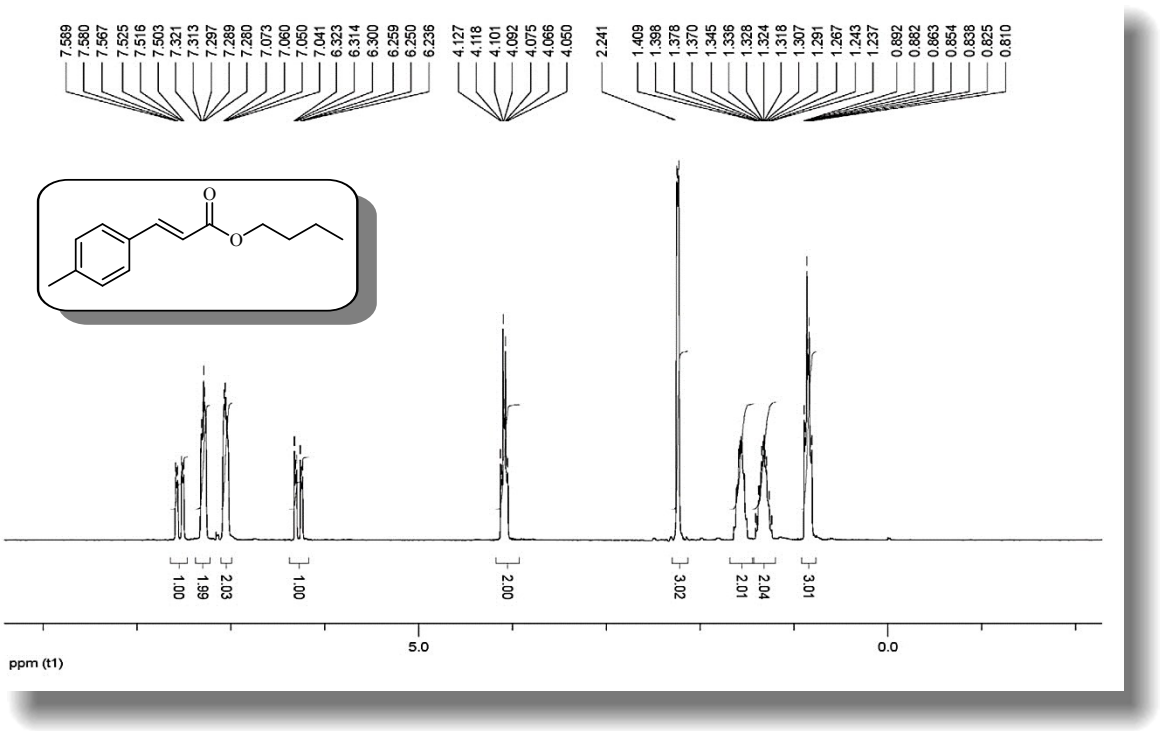

Figure 21-A: ^{1}H NMR (400 MHz, $CDCl_3$) of (*E*)-Butyl 3-(*p*-tolyl) acrylate (2n).

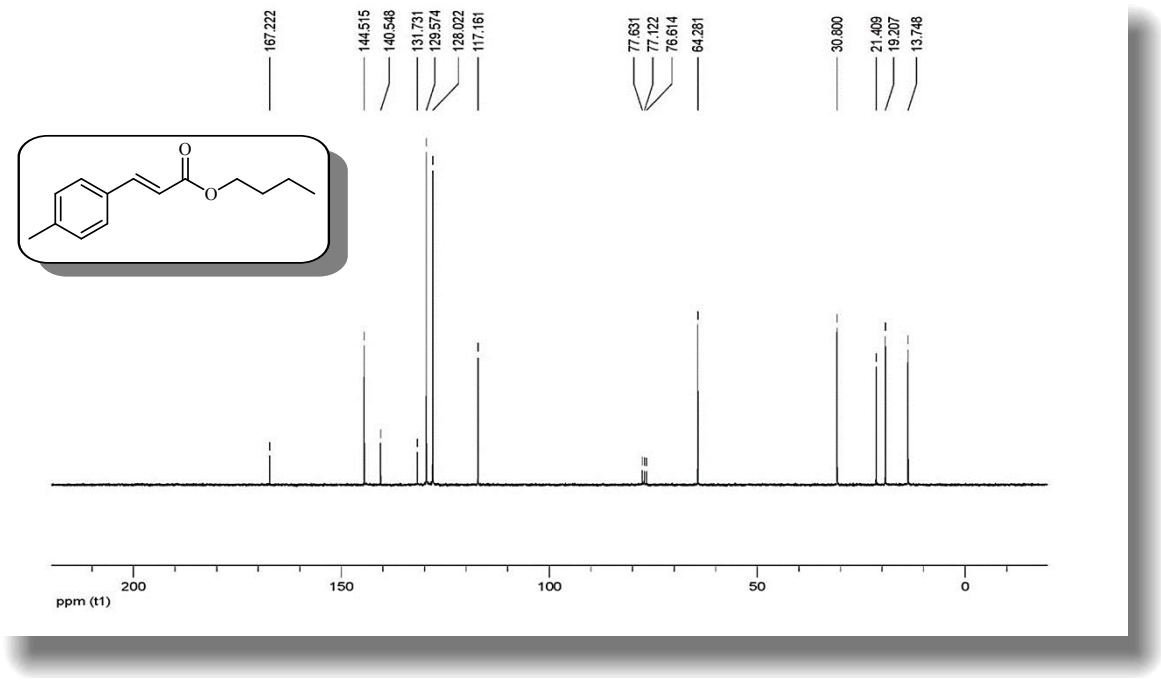

Figure 21-B: ^{13}C NMR (100 MHz, $CDCl_3$) of (*E*)-Butyl 3-(*p*-tolyl) acrylate (2n).

(*E*)-Butyl 3-(thiophen-2-yl)acrylate (2o): [20] Oil; ^{1}H NMR (300 MHz, $CDCl_3$) δ 7.78 (d, *J* = 15.6 Hz, 1H), 7.36 (d, *J* = 4.8 Hz, 1H), 7.25 (d, *J* = 4.5 Hz, 1H), 7.04 (d, *J* = 4.8 Hz, 1H), 6.24 (d, *J* = 15.6 Hz, 1H), 4.20 (t, *J* = 6.6 Hz, 2H), 1.63-1.72 (m, 2H), 1.37-1.49 (m, 2H), 0.94 (t, *J* = 7.2 Hz, 3H); ^{13}C NMR (100 MHz, $CDCl_3$) δ 167.0, 139.6, 137.0, 130.8, 128.3, 128.1, 117.1, 64.4, 30.8, 19.2, 13.7.

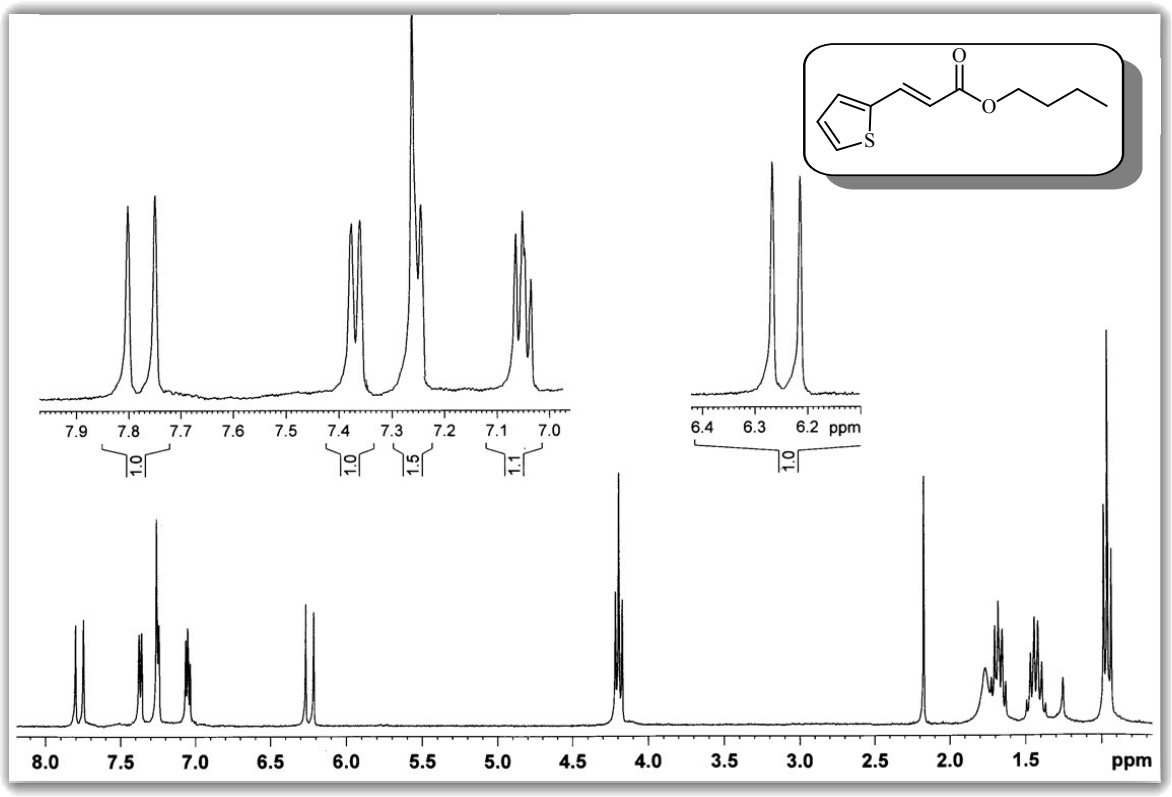

Figure 22-A: ^{1}H NMR (400 MHz, $CDCl_3$) of (*E*)-Butyl 3-(thiophen-2-yl) acrylate (2o).

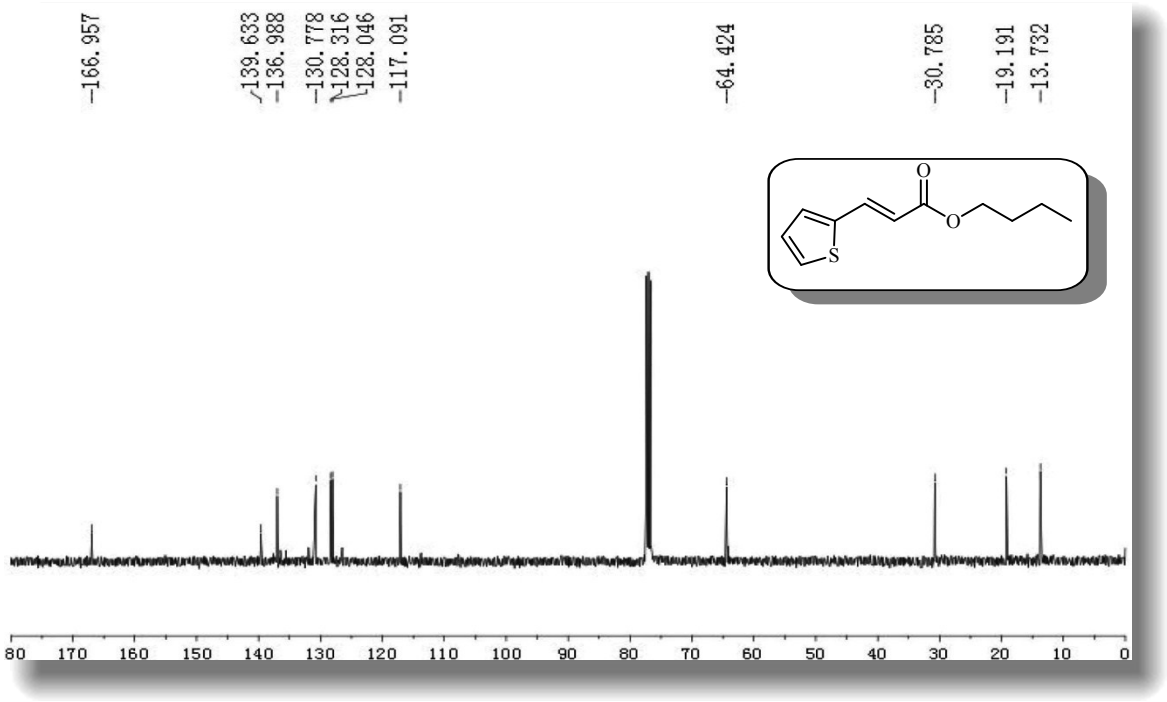

Figure 22-B: ^{13}C NMR (100 MHz, $CDCl_3$) of (*E*)-Butyl 3-(thiophen-2-yl) acrylate (2o).

References:

[1] S. Rostamnia, H. Alamgholiloo and X. Liu, *J. Colloid Interface Sci*., 2016, **469**, 310.

[2] I. Hoffmann, B. Blumenröder, S. O. neé Thumann, S. Dommer and J. Schatz, *Green Chem*., 2015, **17**, 3844.

[3] R. J. Tang, Q. He and L. Yang, *Chem. Commun*., 2015, **51**, 5925.

[4] D. H. Ortgies, A. Barthelme, S. Aly, B. Desharnais, S. Rioux and P. Forgione, *Synthesis*, 2013, **45**, 694.

[5] S. J. Hoseini, M. Dehghani and H. Nasrabadi, *Catal. Sci. Technol*., 2014, **4**, 1078.

[6] R. J. Kalbasi and N. Mosaddegh, *Bull. Korean Chem. Soc*., 2011, **32**, 2584.

[7] X. Li, T. Zhu, Z. Shao, Y. Li, H. Chang, W. Gao, Y. Zhang and W. Wei, *Tetrahedron*, 2016, **72**, 69.

[8] Y. Kawagoe, K. Moriyama and H. Togo, *Eur. J. Org. Chem*., 2014, **2014**, 4115.

[9] A. L. Isfahani, I. Mohammadpoor-Baltork, V. Mirkhani, A. R. Khosropour, M. Moghadam, S. Tangestaninejad and R. Kia, *Adv. Synth. Catal.,* 2013, **355**, 957.

[10] Q. Zhang, H. Su, J. Luo and Y. Wei, *Tetrahedron*, 2013, **69**, 447.

[11] K. S. Nalivela, M. Tilley, M. A. McGuire and M. G. Organ, *Chem. Eur. J*., 2014, **20**, 6603.

[12] J. Zheng and Y. Shen, *Synth. Commun*., 1994, **24**, 2069.

[13] B. Schmidt and R. Berger , *Adv. Synth. Catal*., 2013, **355**, 463.

[14] B. R. Ambler and R. A. Altman , *Org. Lett*., 2013, **15**, 5578.

[15] M. Amini and H. Etemadi, *Chem. Pap*., 2013, **67**, 759.

[16] X. Zhou, J. Luo, J. Liu, S. Peng and G. J. Deng, *Org. Lett*., 2011, **13**, 1432.

[17] N. Iranpoor, H. Firouzabadi, A. Tarassoli and M. Fereidoonnezhad, *Tetrahedron*, 2010, **66**, 2415.

[18] F. Ebrahimzadeh and B. Tamami, *Phosphorus Sulfur Silicon Relat Elem*., 2015, **190**, 144.

[19] P. Cyr, S. T. Deng, J. M. Hawkins and K. E. Price, *Org. Lett*., 2013, **15**, 4342.

[20] W. Yang, H. Chen, J. Li, C. Li, W. Wu and H. Jiang, *Chem. Commun*., 2015, **51**, 9575.